Title

Stromal-derived MAOB promotes prostate cancer growth and progression.

Journal

Science Advances, 10(6)

Authors

Pu, Tianjie

Wang, Jing

Wei, Jing

et al.

Publication Date

2024-02-09

DOI

10.1126/sciadv.adi4935

Peer reviewed

CANCER

Stromal-derived MAOB promotes prostate cancer growth and progression

Tianjie Pu[1], Jing Wang[1]†, Jing Wei[1], Alan Zeng[2], Jinglong Zhang[1]‡, Jingrui Chen[1], Lijuan Yin[3]§, Jingjing Li[1]¶, Tzu-Ping Lin[4,5], Jonathan Melamed[6]#, Eva Corey[7], Allen C. Gao[8], Boyang Jason Wu[1]*

Prostate cancer (PC) develops in a microenvironment where the stromal cells modulate adjacent tumor growth and progression. Here, we demonstrated elevated levels of monoamine oxidase B (MAOB), a mitochondrial enzyme that degrades biogenic and dietary monoamines, in human PC stroma, which was associated with poor clinical outcomes of PC patients. Knockdown or overexpression of MAOB in human prostate stromal fibroblasts indicated that MAOB promotes cocultured PC cell proliferation, migration, and invasion and co-inoculated prostate tumor growth in mice. Mechanistically, MAOB induces a reactive stroma with activated marker expression, increased extracellular matrix remodeling, and acquisition of a protumorigenic phenotype through enhanced production of reactive oxygen species. Moreover, MAOB transcriptionally activates CXCL12 through Twist1 synergizing with TGFβ1-dependent Smads in prostate stroma, which stimulates tumor-expressed CXCR4-Src/JNK signaling in a paracrine manner. Pharmacological inhibition of stromal MAOB restricted PC xenograft growth in mice. Collectively, these findings characterize the contribution of MAOB to PC and suggest MAOB as a potential stroma-based therapeutic target.

INTRODUCTION

Prostate cancer (PC) is the second most commonly diagnosed cancer and the fifth leading cause of cancer death in men worldwide (*1*). Although PC is widely considered to arise by stepwise accumulation of genetic and epigenetic alterations within the epithelial component of the prostatic gland, the surrounding stroma is increasingly recognized as a key contributor to carcinogenesis and cancer progression, including the development of castration-resistant and neuroendocrine (NE) phenotypes and loss of therapeutic responsiveness (*2*–*4*). Induced stromal activation during the tumorigenic process promotes the transformation and growth of epithelial tumor cells. Reprogramming reactive stromal cells, especially cancer-associated fibroblasts (CAFs), the predominant cell type within the tumor microenvironment, has proven feasible for normalizing tumor cells and hampering tumor progression in many experimental cancer models, including PC (*5*, *6*). Despite the therapeutic potential of stroma-based interventions, most current PC therapies focus on tumor cells, resulting in modest to no effectiveness at prolonging the survival of patients with advanced relapsed PC, underscoring the need to develop better strategies targeting stromal cells to complement tumor cell–focused therapies for improved disease control.

Stromal-epithelial interactions dictate PC development and progression via cross-talk, mediated primarily through a wide variety of paracrine signaling molecules from stromal cells to enable epithelial tumor cell acquisition of aggressive properties (*7*). For example, transforming growth factor β (TGFβ) signaling has been shown to play a critical regulatory role in stromal-epithelial interactions during PC tumorigenesis by inducing normal-to-reactive stromal transition and maintaining the protumorigenic status of the remodeled stroma (*8*). CAFs, the most abundant stromal cell population within the tumor microenvironment, are a fundamental source of a complex set of growth factors, cytokines, and chemokines that create a proinflammatory and protumorigenic microenvironment potentiating the malignant behavior of tumor cells. Examples of soluble factors enriched in and released by prostatic CAFs include TGFβ, fibroblast growth factor 10 (FGF10), interleukin-6 (IL-6), C-X-C motif chemokine ligand 12 (CXCL12), and growth differentiation factor 15 (GDF15), which stimulate adjacent tumor growth and invasion (*8*–*11*).

Monoamine oxidases, with two isoforms (MAOA and MAOB), are a pair of mitochondrial outer membrane–bound enzymes that break down a number of biogenic and dietary amines, including monoamine neurotransmitters, and generate hydrogen peroxide (H_2O_2), a reactive oxygen species (ROS), as a byproduct. These isoenzymes differ in cell- and tissue-specific distribution, substrate preference, and inhibitor specificity. By regulating the levels of monoamine neurotransmitters, such as serotonin and dopamine, MAO enzymes contribute to modulation of mood, behavior, and cognition in humans. The small-molecule MAO inhibitors, used either selectively against individual enzymes or nonselectively against both enzymes, are currently in clinical use for treating neurological disorders such as depression (*12*, *13*). Beyond their brain functions,

[1]Department of Pharmaceutical Sciences, College of Pharmacy and Pharmaceutical Sciences, Washington State University, Spokane, WA 99202, USA. [2]Undergraduate Programs, University of Washington, Seattle, WA 98195, USA. [3]Uro-Oncology Research Program, Samuel Oschin Comprehensive Cancer Institute, Department of Medicine, Cedars-Sinai Medical Center, Los Angeles, CA 90048, USA. [4]Department of Urology, Taipei Veterans General Hospital, Taipei 11217, Taiwan, Republic of China. [5]Department of Urology, School of Medicine and Shu-Tien Urological Research Center, National Yang Ming Chiao Tung University, Taipei 11221, Taiwan, Republic of China. [6]Department of Pathology, Grossman School of Medicine, New York University, New York, NY 10016, USA. [7]Department of Urology, University of Washington, Seattle, WA 98195, USA. [8]Department of Urologic Surgery, University of California, Davis, Sacramento, CA 95817, USA.
*Corresponding author. Email: boyang.wu@wsu.edu
†Present address: Department of Medical Oncology, Dana-Farber Cancer Institute, Boston, MA 02215, USA.
‡Present address: Department of Genetics and Genomic Sciences, Icahn School of Medicine at Mount Sinai, New York, NY 10029, USA.
§Present address: Department of Pathology, West China Hospital, Sichuan University, Chengdu, Sichuan 610041, China.
¶Present address: Engineering Research Center of Cell & Therapeutic Antibody, School of Pharmacy, Shanghai Jiao Tong University, Shanghai 200240, China.
#Present address: Department of Pathology, NYU Long Island School of Medicine, Mineola, NY 11501, USA.

we and others previously demonstrated that MAOA expressed in PC tumor epithelial cells and associated stromal cells is up-regulated throughout the disease course and plays an essential role mediating PC tumorigenesis, growth, progression, and metastasis (*14*–*16*). However, the function and clinical relevance of MAOB in PC remain unclear. Here, we address the role of MAOB in the stromal fibroblasts in PC pathogenesis and progression.

RESULTS

MAOB expression levels are elevated in PC stroma

To seek initial evidence of MAOB's role in PC, we assessed MAOB protein levels in a commercial tissue microarray (TMA) from US Biomax, including primary human PC ($n = 97$) and normal human prostate tissues ($n = 12$), by immunohistochemistry (IHC). We found higher MAOB expression in stromal cells compared to adjacent epithelial cells in cancerous tissues (fig. S1A), where the stroma was recognized as a cell population expressing α smooth muscle actin (αSMA; encoded by *ACTA2*) as stained on a separate serial section of TMA by IHC. In contrast to decreased MAOB expression in the epithelial cells of cancerous relative to normal prostate tissues (fig. S1B), we found elevated levels of both MAOB and αSMA in tumor-associated stroma compared to normal prostate stroma (Fig. 1A). We also costained the TMA for MAOB and αSMA by immunofluorescence (IF) and confirmed increased MAOB expression in the αSMA^+ cells of tumor versus normal tissues (fig. S1C). On the basis of these findings, we speculated that the higher MAOB expression in the tumor stroma is more likely to have an effect in PC compared to MAOB expressed in the epithelium, leading us to focus on stromal MAOB's role in PC in this study. Next, we assessed the association of stromal MAOB with PC progression using TMAs from two independent cohorts [US Biomax and New York University (NYU)], where tumor samples were categorized on the basis of high Gleason scores (GS 7 to 10) versus low Gleason scores (GS 4 to 6). IHC analysis of MAOB and αSMA in serial sections of individual TMAs revealed increased expression of MAOB and αSMA in the αSMA^+ tumor stroma upon progression to aggressive, poorly differentiated high-grade stage PC in both cohorts (Fig. 1, B and C). Costaining the US Biomax TMA with MAOB and αSMA by IF also demonstrated up-regulated MAOB expression in the αSMA^+ stromal cells of high- versus low-GS PC, accompanied by a positive correlation between MAOB and αSMA expression in the αSMA^+ stroma (fig. S1D).

To further compare the expression patterns of MAOA and MAOB in PC epithelial and stromal cells, we performed a co-IF assay to simultaneously visualize both MAOs in the US Biomax TMA. We demonstrated a higher level of MAOA than MAOB in epithelial tumor cells and a greater abundance of MAOB than MAOA in stromal cells. Moreover, MAOA had increased expression in tumor cells relative to stromal cells, while MAOB was more present in stromal cells than tumor cells (fig. S2A). In contrast to the elevated expression of MAOA in the tumor cells of high- versus low-GS PC, which recapitulated the previous findings from others and us (*14*, *15*), MAOB expression in tumor cells was not altered by GSs. On the other hand, both MAOA and MAOB demonstrated higher expression levels in the stromal cells of high- versus low-GS PC, which was consistent with the above and our previously reported findings (fig. S2B) (*16*). Given recent studies indicating gene expression and phenotypic and functional heterogeneities in CAFs (*17*, *18*), we also examined the expression patterns of MAOA

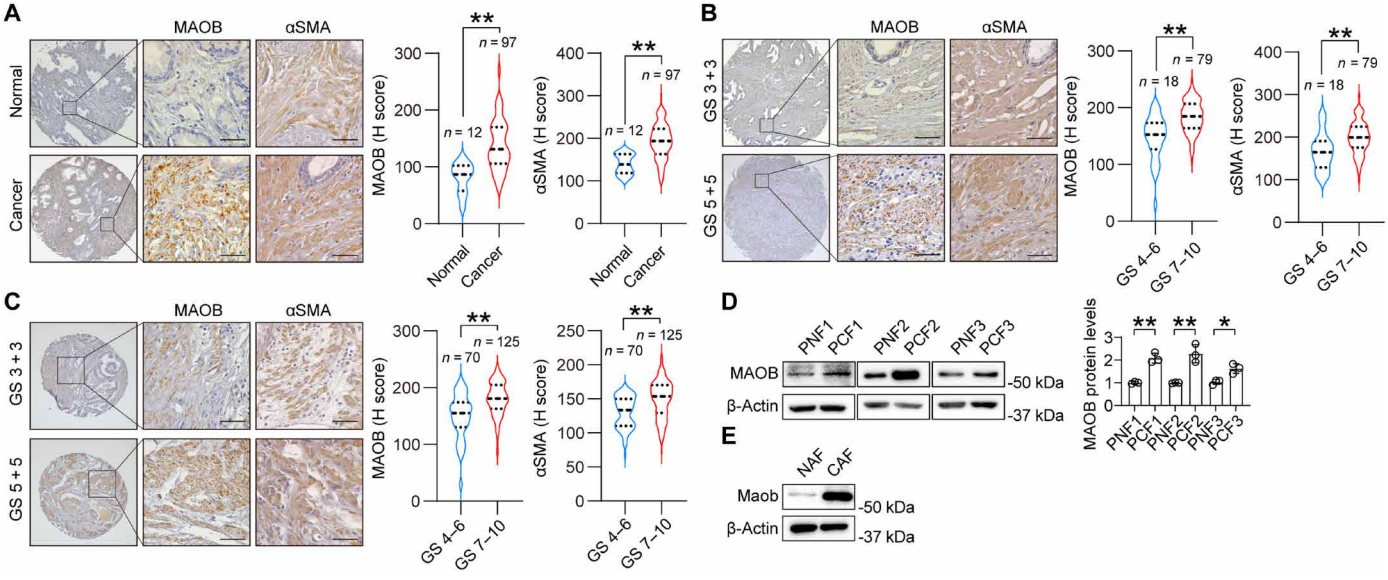

Fig. 1. MAOB levels are elevated in the stroma of human PC. (**A**) Representative images and quantitation of MAOB and αSMA IHC staining in the stroma of normal prostates ($n = 12$) and PC ($n = 97$) from a US Biomax TMA. Scale bars, 50 μm. (**B**) Representative images and quantitation of MAOB and αSMA IHC staining in the stroma along with PC progression categorized by low GS (4 to 6, $n = 18$) and high GS (7 to 10, $n = 79$) from the TMA in (A). Scale bars, 50 μm. (**C**) Representative images and quantitation of MAOB and αSMA IHC staining in the stroma along with PC progression categorized by low GS ($n = 70$) and high GS ($n = 125$) from the NYU TMA. Scale bars, 50 μm. (**D**) Western blot of MAOB and its quantitation from three independent blots of three matched pairs of PC patient–derived fibroblasts, normal prostate fibroblasts (PNFs), and PC-associated fibroblasts (PCFs). (**E**) Western blot of MAOB in NPFs and CAFs derived from WT mouse prostates and Pten-KO mouse prostate tumors, respectively. Statistical analysis was performed using unpaired Student's *t* test. Data represent means ± SEM. $^*P < 0.05$, $^{**}P < 0.01$.

and MAOB in different CAF subsets. To this end, we collected single-cell RNA sequencing (RNA-seq) data for 13 primary PC samples and 6 castration-resistant PC (CRPC) samples from two public datasets (GSE141445 and GSE137829). By distinguishing 1518 and 1144 fibroblast cells from the primary PC and CRPC cohorts, respectively, as three well-established CAF subsets, including myofibroblast-like CAF (myCAF), inflammatory CAF (iCAF), and antigen-presenting CAF (apCAF), using corresponding biomarkers (myCAF: *ACTA2*, *RSG5*, *POSTN*, and *TAGLN*; iCAF: *CCL2*, *CXCL12*, and *IL6*; apCAF:*CD74* and *HLA-DRA*) (*17*, *18*), we found that the fibroblasts from both primary PC and CRPC were mainly composed of myCAFs with limited iCAFs and absent apCAFs (fig. S2, C and D). Next, we assessed MAOA and MAOB levels in individual CAF subsets from a small portion of fibroblast cells with detectable MAOA and/or MAOB transcripts, up to 119 and 106 cells from primary PC and CRPC, respectively. MAOA expression had no significant changes between myCAFs and iCAFs of both primary PC and CRPC. MAOB expression remained invariable between myCAFs and iCAFs of primary PC but was up-regulated in iCAFs relative to myCAFs of CRPC (fig. S2E).

Examining three matched pairs of PC patient-derived primary fibroblasts as established and characterized in a prior report (*19*), we demonstrated 58 to 128% higher MAOB protein levels, increases with statistical significance, in CAFs (PCF1, PCF2, and PCF3) compared to their counterparts, adjacent normal prostate-associated fibroblasts (PNF1, PNF2, and PNF3) (Fig. 1D). We also revealed up-regulated MAOB protein expression in mouse CAFs from prostate tumors developed in prostate-specific Pten-knockout (KO) mice compared to normal prostate fibroblasts (NPFs) from wild-type (WT) mice (Fig. 1E). We then examined MAOB response to select well-established activating signals for CAF generation and activation, as exemplified by inflammatory modulators, which are released from tumor cells including PC cells during tumor-stroma coevolution (*18*, *20*–*23*). We demonstrated induction of *MAOB* and select CAF markers [fibroblast activation protein (*FAP*) and vimentin (*VIM*)] at the mRNA level upon treatment with tumor necrosis factor α (TNFα) and IL-6 but not IL-1α in normal human prostate fibroblast prostate stromal cells (PrSC) cells (fig. S1E). These data provided clues for potential upstream cues and signaling mechanisms [e.g., TNFα–nuclear factor κB (NF-κB) and IL-6–signal transducer and activator of transcription 3 (STAT3)] for MAOB up-regulation in CAFs, which merits additional investigation. Collectively, these results suggested the potential association of stromal MAOB with PC tumorigenesis and progression.

Up-regulated MAOB levels in the stroma are associated with worse clinical outcomes in PC

To determine the association of stromal MAOB with additional clinical indicators along the disease trajectory, we first examined stromal MAOB protein expression in a tissue panel including hormone-naïve PC (HNPC) and CRPC by IHC and found higher MAOB levels in the stroma of CRPC (n = 16) relative to HNPC (n = 38) (Fig. 2A). NE differentiation has been shown to emerge and expand along disease progression toward high-grade and high-stage

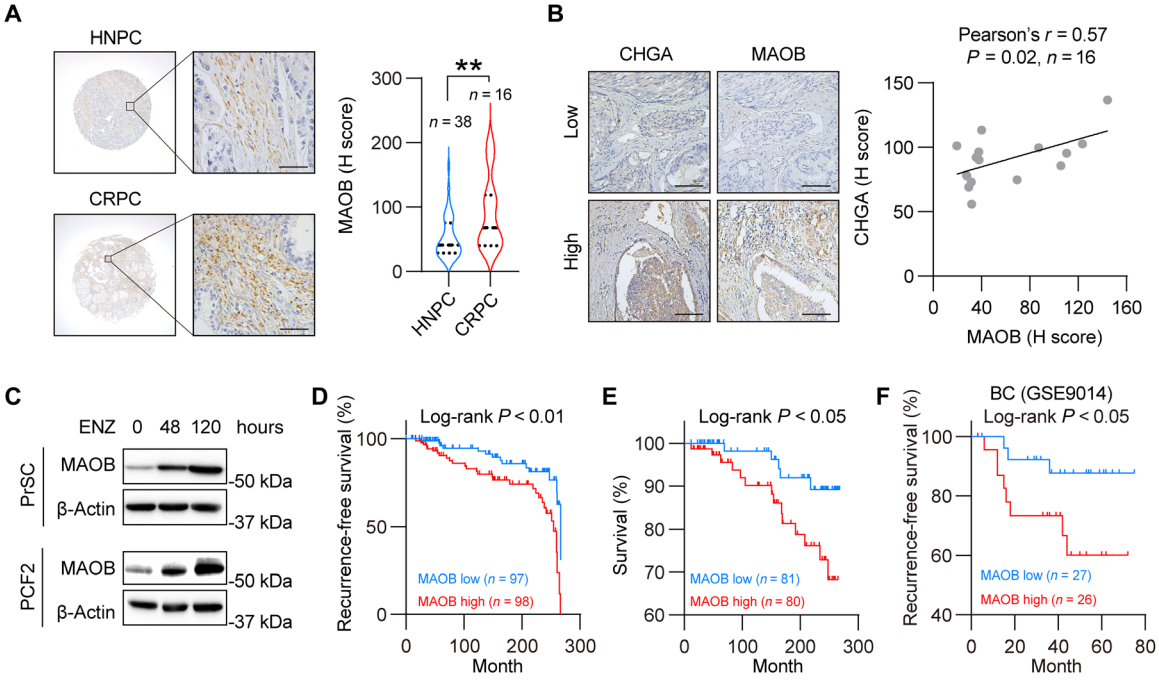

Fig. 2. MAOB up-regulation in the tumor stroma is associated with worse clinical outcomes in PC patients. (**A**) Representative images and quantitation of MAOB IHC staining in the stroma of hormone-naïve (HNPC, n = 38) and castration-resistant (CRPC, n = 16) PCs. Scale bars, 50 μm. (**B**) Representative images and corresponding Pearson's correlation analysis of stromal MAOB and adjacent epithelial CHGA expression from the CRPC cohort (n = 16) in (A). Scale bars, 100 μm. (**C**) Western blot of MAOB in PrSC and PCF2 cells upon ENZ treatment (20 μM) at indicated times. (**D** and **E**) Kaplan-Meier recurrence-free (D, n = 195) and cancer-specific (E, n = 161) survival curves of PC patients from the NYU cohort with either low or high stromal MAOB protein levels. (**F**) Kaplan-Meier recurrence-free survival curves of BC patients from GSE9014 with either low or high *MAOB* mRNA levels in the tumor stroma. Statistical analysis was performed using unpaired Student's *t* test in (A) and log-rank test in (D) to (F). Data represent means ± SEM. **P < 0.01.

PC tumors, particularly upon androgen deprivation therapy as a treatment-induced response, which correlates with adverse clinical outcomes (*24*, *25*). Using the NE marker chromogranin A (CHGA) for assessing the extent of NE differentiation in CRPC tumors, we found a positive correlation between stromal MAOB and adjacent tumor CHGA protein expression in CRPC samples (Pearson's $r = 0.57$, $P = 0.02$, $n = 16$) (Fig. 2B). To consolidate this finding in a different cohort with additional NE markers, we demonstrated a positive relationship of protein levels between stromal MAOB and two NE markers (CHGA and SYP) in adjacent tumor cells in a human primary PC TMA ($n = 40$) including high-grade PC by multiplex IF staining (CHGA: Pearson's $r = 0.49$, $P = 0.001$; SYP: Pearson's $r = 0.90$, $P < 0.001$) (fig. S3A). To recapitulate these findings in vitro, we determined whether cancer cell–focused anti–androgen receptor (AR) therapy has a direct effect on stromal MAOB. To this end, we treated AR-expressing PrSC and PCF2 cells (*26*) with enzalutamide (ENZ), an AR inhibitor used clinically for CRPC management and able to induce a NE phenotype (*27*). Systemic administration of ENZ is considered to also modulate the stromal AR signaling that plays a role in PC tumorigenesis and progression as reported previously (*28*, *29*). PCF2 was selected as a representative primary human prostatic CAF cell line, which had the utmost MAOB up-regulation compared to its normal counterpart among three fibroblast pairs (Fig. 1D). We showed that ENZ time-dependently increased MAOB protein expression in both PrSC and PCF2 cells (Fig. 2C), suggesting that MAOB up-regulation may be a stromal response to anti-AR therapy in PC. We also demonstrated that ENZ enhanced *MAOB* mRNA level in PrSC cells, but we did not identify any obvious AR-binding peaks at the *MAOB* gene locus by interrogating existing AR chromatin immunoprecipitation (ChIP) sequencing data obtained in human prostate fibroblast cells (GSE90772) (fig. S3, B and C). These data suggested that AR is likely to regulate MAOB expression indirectly in stromal fibroblasts, which warrants further investigation.

Correlating stromal MAOB protein levels with clinical attribute data procured from the NYU cohort, we further demonstrated that high-stromal MAOB patients had significantly greater incidence of recurrence (log-rank $P < 0.01$) and shorter cancer-specific survival times (log-rank $P < 0.05$) compared to low-stromal MAOB patients (Fig. 2, D and E). In contrast, tumor epithelial MAOB expression was not found to be associated with disease recurrence and survival in the same cohort (fig. S3, D and E). We also interrogated a breast cancer (BC) clinical dataset (GSE9014) and found that BC patients with high stromal *MAOB* mRNA expression had a significantly greater incidence of recurrence (log-rank $P < 0.05$) compared to those with low expression (Fig. 2F). Together, these data indicated the clinical relevance and importance of stromal MAOB in PC.

Stromal MAOB promotes PC cell proliferation, invasion, and tumor growth

To test whether stromal MAOB influences PC cell behavior and associated properties, we first stably overexpressed or knocked down MAOB in PrSC cells proven suitable for use to investigate stromal-epithelial cell interactions in PC based on prior reports including ours (*16*, *30*, *31*) (Fig. 3A). Parallel stable introduction of an empty vector or a scrambled short hairpin RNA (shRNA) into PrSC cells as controls did not alter endogenous MAOB expression as compared to parental cells (fig. S4A). To determine the role of MAOB silencing in normal stroma, we performed a series of cell health assays with PrSC and PNF1 cells, where PNF1 was selected as a representative primary normal fibroblast cell line. With comparable *MAOB* levels expressed between PrSC and PNF cells (fig. S4B), we found that knocking down MAOB caused no toxicity to PrSC and PNF1 cells, with negligible changes in cell cycle and cell viability, proliferation, and apoptosis (fig. S4, C to G). We set up a two-dimensional (2D) cell coculture model growing PC cells expressing luciferase (Luc) or a fluorescence protein over a monolayer of fibroblast cells. A panel of aggressive human PC cell lines with different AR status and ENZ responsiveness was selected for cocultures, including C4-2 (AR-positive CRPC), PC-3 (AR-negative CRPC), DU145 (AR-negative CRPC), and C4-2B^{ENZR} [AR-indifferent ENZ-resistant CRPC with acquired NE traits (*32*, *33*)]. Coculturing different PC cells with PrSC cells, we showed up to a 6.3-fold increase or 79% decrease in cancer cells when MAOB overexpression (OE) or knockdown (KD) was executed, respectively, in PrSC cells compared to controls (Fig. 3, B and C). Treating PC cells with conditioned media (CM) from control and MAOB-manipulated PrSC cells corroborated these findings (Fig. 3D). Applying a 3D organotypic cell coculture model validated in multiple types of cancer including PC (*8*, *34*–*36*), we demonstrated increased or reduced proliferation of PC-3 cells when cocultured with MAOB-OE or KD human fibroblasts, respectively, compared to controls (Fig. 3E). Consistent with the observations in human cell cultures, ablating Maob in mouse CAFs also decreased proliferation of cocultured mouse PC MPC3 and TRAMP-C2 cells compared to controls (fig. S5, A and B). Moreover, we established a transwell-based coculture model with cancer cells added inside transwell inserts, while fibroblast cells were seeded into the bottom of lower chambers, and showed that OE or KD of MAOB in PrSC cells, respectively, enhanced or repressed the invasiveness of C4-2 and PC-3 cells compared to controls (Fig. 3F). Complementing the shRNA-based stable silencing approach, we generated and cocultured PrSC cells expressing a doxycycline (Dox)–inducible *MAOB* shRNA with PC cells and demonstrated reduced proliferation and invasion of C4-2 and PC-3 cells in cocultures upon Dox stimulation for stromal depletion of MAOB (fig. S5, C to E). Furthermore, we enforced MAOB expression in three PNF cell lines, silenced MAOB in three PCF cell lines, and revealed similar results in epithelial proliferation and invasion from cell co-cultures (fig. S5, F to K). In addition, the growth of organoids derived from LuCaP 147CR and LuCaP 93 PC patient-derived xenograft (PDX) tumors, which have castration-resistant and NE features (*37*), was enhanced or repressed, respectively, upon treatment with media conditioned by MAOB-OE PNF1 or MAOB-KD PCF2 as representatives of primary fibroblasts compared to controls (Fig. 3G).

Given the association of stromal MAOB with PC progression, as seen in CRPC, we sought to examine stromal MAOB's effect on anti-AR therapy response, NE differentiation, and other established mechanisms for therapy resistance. To this end, we first showed that treatment with CM of MAOB-OE PrSC cells reduced ENZ efficacy in C4-2 cells, while C4-2B^{ENZR} cells had increased sensitivity to ENZ in the presence of CM of MAOB-KD PrSC cells, compared to controls (fig. S6A). Moreover, we found that treatment with MAOB-OE PrSC CM induced a NE-like differentiated cell morphology with increases in per-cell number of neurites and average neurite lengths, accompanied by up-regulation of several NE markers (CHGA, SYP, CD56, and NSE), in C4-2 and DU145 cells compared to controls (fig. S6, B to D). In addition to triggering a NE phenotype, alternative

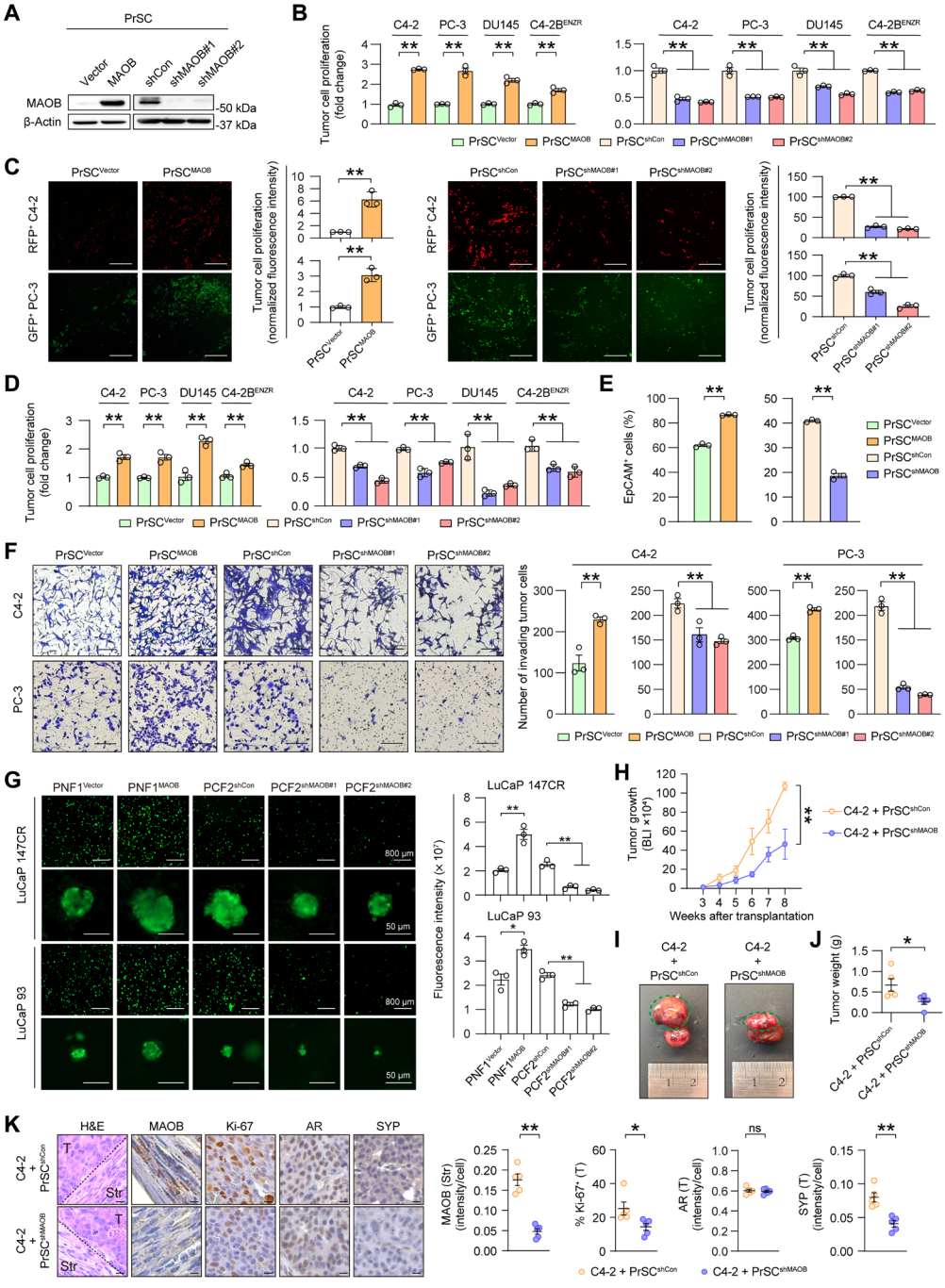

Fig. 3. Stromal MAOB promotes PC cell proliferation, invasion, and tumor growth. (**A**) Western blot of MAOB in control and MAOB-OE/MAOB-KD PrSC fibroblasts. (**B**) Quantitation of PC cells in 2D coculture with control and MAOB-manipulated PrSC cells by Luc assays ($n = 3$). (**C**) Representative fluorescence images and quantitation of green fluorescent protein (GFP)–tagged PC-3 or red fluorescent protein (RFP)–tagged C4-2 cells in 2D coculture with control and MAOB-manipulated PrSC cells by fluorescence microscopy ($n = 3$). Scale bars, 100 μm. (**D**) Quantitation of PC cells incubated with CM from control and MAOB-manipulated PrSC cells for 3 to 5 days ($n = 3$). (**E**) Quantitation of EpCAM$^+$ cancer epithelium in 3D cocultures of PC-3 cells with control and MAOB-manipulated PrSC cells by flow cytometry ($n = 3$). (**F**) Representative images and quantitation of invasive PC cells in transwell-based coculture with control and MAOB-manipulated PrSC cells ($n = 3$). Scale bars, 200 μm. (**G**) Representative fluorescence images and quantitation of LuCaP 147CR and LuCaP 93 PC PDX–derived organoids after 14-day incubation with CM from control and MAOB-manipulated primary fibroblasts ($n = 3$). Scale bars, 50 or 800 μm. (**H**) BLI-based growth curves of subrenal capsule xenografts combining Luc-tagged C4-2 cells with control or MAOB-KD PrSC cells in male SCID mice ($n = 5$). (**I**) Representative anatomical images of tumor-grown mouse kidneys from each group. Green dashed circles denote size of tumor outgrowth from renal capsules. (**J**) Tumor weights from each group ($n = 5$). (**K**) Representative images of hematoxylin and eosin (H&E) and IHC staining of stromal (Str) MAOB and tumor (T) Ki-67, AR, and SYP and their quantitation in tumor samples from each group ($n = 5$). Scale bars, 10 μm. Statistical analysis was performed using unpaired Student's *t* test for comparisons between two groups and one-way analysis of variance (ANOVA) with Dunnett's test for comparisons between three groups in (B) to (F), (G), (J), and (K), and two-way ANOVA with Sidak's test in (H). Data represent means ± SEM. $^*P < 0.05$, $^{**}P < 0.01$; ns, not significant.

mechanisms by which PC cells evade anti-AR therapy such as ENZ have been reported, including promotion of AR variants/mutants with constitutive activity, conversion to glucocorticoid receptor (GR) dependence, induction of androgen biosynthetic and metabolic pathways, and activation of master regulators driving lineage plasticity toward a stemness and multilineage state without necessarily involving a NE lineage (*38*–*41*). We demonstrated down-regulated mRNA levels of *AR* variants, *GR*, androgen biosynthetic and metabolic pathway genes, and master regulators and lineage markers associated with multiple cell lineages (NE, basal, stemness and multilineage, and mesenchymal) in C4-2B^{ENZR} cells exposed to MAOB-KD PrSC CM compared to controls (fig. S6E). Conversely, treating C4-2 cells with MAOB-OE PrSC CM resulted in the opposite expression changes of these genes compared to controls (fig. S6F). These data suggested that stromal MAOB may use diverse mechanisms to contribute to anti-AR therapy resistance in PC.

To investigate the in vivo consequences of MAOB expression in the tumor stroma, we admixed Luc-tagged C4-2 cells with control or MAOB-KD PrSC fibroblasts as recombinant tissue grafts and transplanted the grafts under the renal capsule of immunodeficient male mice. We showed that MAOB KD in PrSC cells markedly slowed tumor growth in mice (Fig. 3H). Eight weeks after implantation, C4-2 grafts grew to a substantially smaller size in the presence of MAOB-KD fibroblasts compared to those with control fibroblasts (Fig. 3, I and J). Continued MAOB silencing in fibroblasts as confirmed by IHC yielded a 43% decrease of Ki-67$^+$ tumor cells and 49% lower tumor expression of SYP with no significant changes in tumor AR expression compared to controls (Fig. 3K). To further assess mouse fibroblast infiltrates likely to be recruited into human tumor xenografts, we measured mRNA levels of several stromal markers (*Acta2*, *Rgs5*, *Dcn*, *Itga2*, and *Plaur*) in xenograft samples using mouse-specific primers. Our data revealed the presence of tumor-infiltrating mouse fibroblasts based on the mouse stromal gene expression detected. The mouse fibroblasts found in tumor xenografts grown with MAOB-KD PrSC cells demonstrated prevalently lower levels of stromal markers, indicative of either fewer mouse fibroblast infiltrates or less stromal reactivity of mouse fibroblasts, compared to controls (fig. S7A). In addition, we co-inoculated tumorigenic C57BL/6 syngeneic mouse PC Pten-KO/Kras-OE cells with control or Maob-KD mouse CAFs subcutaneously into C57BL/6 immunocompetent male mice. Similarly, we observed smaller tumors associated with lower weight and less percentage of Ki-67$^+$ tumor cells from the groups with Maob-KD CAFs relative to controls at the end point (fig. S7, B to D).

Our recent findings have shown that up-regulated MAOA in stromal cells can promote PC by enhancing ROS production via oxidative enzymatic reactions and activating paracrine IL-6 signaling (*16*). Since MAOB and MAOA are isoenzymes with similar functions, we sought to elucidate whether MAOA is involved in MAOB modulation and function in stromal cells. We demonstrated that neither OE nor KD of MAOB changed MAOA and IL-6 protein expression and MAOA enzymatic activity in PrSC or PCF2 cells (fig. S8, A and B). Moreover, IHC analysis revealed stable MAOA levels in both epithelial and stromal compartments of C4-2 xenograft tumors grown with MAOB-silenced PrSC fibroblasts compared to control tumors (fig. S8C). These data support the finding that MAOB functions independently from MAOA in stromal cells. In all, we concluded that MAOB up-regulation in stromal fibroblasts has a pivotal role supporting PC growth and invasion.

MAOB induces stromal reactivity by activation of ROS-dependent transition toward a CAF phenotype

Considering our above findings that stromal MAOB stimulates PC cell proliferation and invasion, we speculated that stromal MAOB activation may enable stromal reprogramming to a reactive state for epithelial acquisition of aggressive properties. We carried out transcriptome profiling of MAOB-OE versus control PrSC fibroblasts. Gene set enrichment analysis (GSEA) identified positive enrichment of the "response to wounding" gene signature from the gene ontology (GO) gene set library in MAOB-OE fibroblasts (Fig. 4A). Because CAFs exhibit an "activated phenotype" during tumor progression that mirrors fibroblasts during the wound-healing process (*2*, *8*), this result suggested that activated MAOB-high stroma likewise has a more CAF-like phenotype than normal controls. To prove this idea, we first examined MAOB's effect on αSMA and TGFβ1 expression, two bona fide markers of the CAF phenotype (*2*), in fibroblasts. We found that MAOB OE induced, while MAOB KD repressed, αSMA protein expression in PrSC cells (Fig. 4B), which was paralleled by a decrease in αSMA IHC staining, indicative of less reactive stroma, in sections from C4-2 tumors grown with MAOB-KD PrSC fibroblasts relative to controls (Fig. 4C). We showed that MAOB OE increased, while MAOB silencing reduced, the secretion of TGFβ1 as well as the phosphorylation levels of Smad2 and Smad3 proteins, the principal downstream effectors of TGFβ signaling, in PrSC cells (Fig. 4, D and E). MAOB KD also down-regulated TGFβ1 and Smad2/Smad3 phosphorylation in PCF2 cells (fig. S9, A and B). Consistent with this, GSEA revealed positive and negative enrichment of an activated TGFβ signaling target gene signature in MAOB-OE and KD PrSC cells, respectively (Fig. 4F). In addition, we demonstrated the same trend of changes in the mRNA levels of several reactive stromal markers (*ACTA2*, *TGFB1*, *FAP*, and *VIM*) upon either OE or KD of MAOB in PNFs and PCFs, respectively (fig. S9, C and D).

Next, we questioned how MAOB promotes the formation of reactive stroma. Following previous observations of oxidative stress as an inductive mechanism contributing to the development of reactive stroma in PC (*8*, *42*), we hypothesized that MAOB may cause stromal activation through ROS generation as an oxidative enzyme. Testing this possibility, we found a 57% drop in intracellular ROS levels in MAOB-KD PrSC cells compared to controls (Fig. 4G). Concordantly, GSEA revealed two ROS-dependent gene signatures for "reactive oxygen species pathway" and "cellular response to reactive oxygen species" in the Hallmark and GO gene set libraries, respectively, negatively enriched in MAOB-silenced PrSC cells (Fig. 4H). To determine whether ROS mediates MAOB's effect on stromal reactivity, we found that *N*-acetylcysteine (NAC), a ROS scavenger, reversed MAOB OE–induced αSMA protein expression in PrSC cells, while addition of H_2O_2, the direct ROS byproduct of MAOB-mediated enzymatic reaction, rescued αSMA protein levels repressed by MAOB silencing in PrSC cells (Fig. 4I). Similar findings were also demonstrated on the expression patterns of additional reactive stromal markers, such as *TGFB1*, *FAP*, and *VIM*, under the identical conditions in PrSC cells (Fig. 4J). To further establish that MAOB induces a reactive stroma through ROS, we generated a MAOB (Y435S) active site mutant construct deficient in enzymatic activity as reported previously (*43*). Forced expression of MAOB (Y435S) mutant, resulting in a complete loss of enzymatic activity and associated ROS production, failed to induce the expression of several reactive stromal markers in PrSC cells compared to the WT counterpart (fig. S9, E to G).

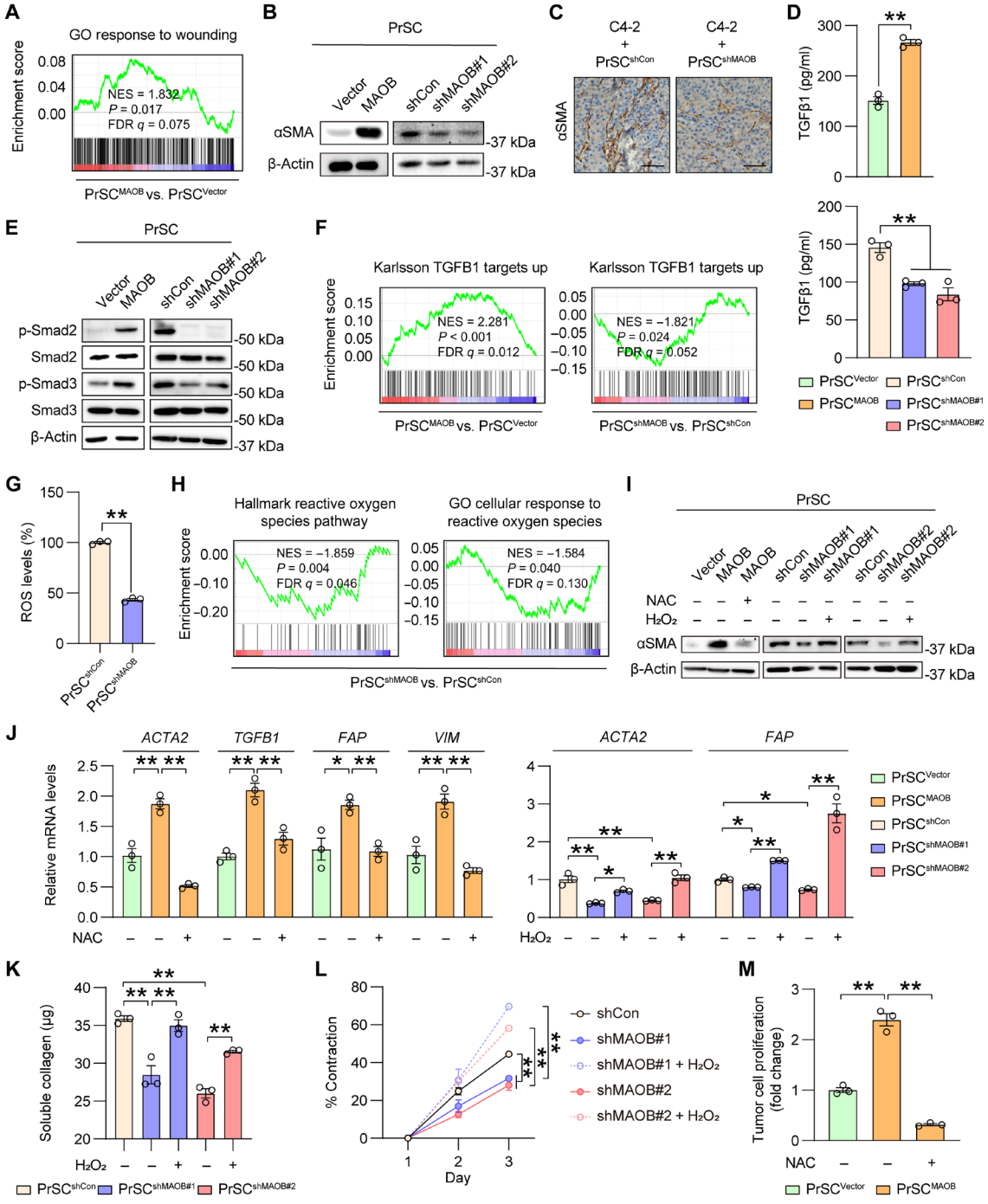

Fig. 4. MAOB induces development of reactive stroma in a ROS-dependent manner. (**A**) GSEA plot of "response to wounding" gene signature enriched in MAOB-OE PrSC cells versus controls. (**B**) Western blot of αSMA in control and MAOB-OE/MAOB-KD PrSC cells. (**C**) Representative αSMA IHC staining of C4-2 tumors co-inoculated with control or MAOB-KD fibroblasts in mice. Scale bars, 100 μm. (**D**) Enzyme-linked immunosorbent assay (ELISA) of TGFβ1 secretion in the culture media of control and MAOB-manipulated PrSC cells ($n = 3$). (**E**) Western blot of p-Smad2 and p-Smad3 in control and MAOB-manipulated PrSC cells. (**F**) GSEA plots of "TGFβ1 targets up" gene signature enriched in MAOB-manipulated PrSC cells versus controls. (**G**) Quantitation of intracellular ROS levels in control and MAOB-KD PrSC cells ($n = 3$). (**H**) GSEA plots of two ROS-related gene sets enriched in MAOB-KD PrSC cells versus controls. (**I**) Western blot of αSMA in control and MAOB-manipulated PrSC cells upon NAC (5 mM, 48 hours) or H_2O_2 treatment (40 μM, 24 hours). (**J**) qPCR of indicated reactive stromal markers in control and MAOB-manipulated PrSC cells upon NAC (5 mM, 48 hours) or H_2O_2 treatment (40 μM, 24 hours) ($n = 3$). (**K** and **L**) Determination of collagen levels deposited (K) and collagen-based cell contraction (L) in control and MAOB-KD PrSC cells under H_2O_2 treatment (40 μM, 24 hours) ($n = 3$). (**M**) Quantitation of PC-3 cells in coculture with control and MAOB-OE PrSC cells pretreated with NAC (5 mM, 24 hours) ($n = 3$). Statistical analysis was performed using unpaired Student's *t* test for comparisons between two groups and one-way ANOVA with Dunnett's test for comparisons between three groups in (D) and (G); one-way ANOVA with Tukey's test in (J), (K), and (M); and two-way ANOVA with Tukey's test in (L). Data represent means ± SEM. $^*P < 0.05$, $^{**}P < 0.01$.

We also assessed the effects of MAOB and ROS on extracellular matrix (ECM) deposition and remodeling since reactive stroma like CAFs secrete increased levels of ECM molecules, including collagens, and modify the stromal ECM to enhance cancer cell migration and invasion (*44*). To this end, we performed a collagen deposition assay and found that MAOB KD reduced collagen accumulation in PrSC cells, which was restored to control levels upon addition of H_2O_2 (Fig. 4K). We also performed a collagen gel contraction assay and demonstrated that MAOB-KD PrSC cells had decreased activity in collagen contraction over controls, which was enhanced by H_2O_2 treatment (Fig. 4L). To determine whether ROS mediates MAOB's effects creating a protumorigenic stromal cell phenotype, we treated MAOB-OE PrSC cells with NAC before setting up cell cocultures with PC-3 cells and found that NAC pretreatment remarkably attenuated epithelial proliferation accelerated by cocultured MAOB-high PrSC cells compared to controls (Fig. 4M). Together, these results suggested that MAOB reprograms the stroma by triggering a CAF phenotype in a ROS-dependent manner.

MAOB activates CXCL12 through Twist1 synergizing with TGFβ signaling in prostate stroma

Having demonstrated the tumor-supportive role of stromal MAOB in PC, we sought to explore the underlying molecular mechanism. Since we demonstrated that epithelial proliferation could be influenced by treatment with stromal cell CM in a stromal MAOB–dependent manner, we speculated that MAOB may function via downstream secreted protein factors to trigger paracrine signaling to engage in stromal-epithelial cross-talk. To test this hypothesis, we first subjected the transcriptome profiling data from MAOB-OE versus control PrSC cells to GSEA using the gene sets from the Kyoto Encyclopedia of Genes and Genomes (KEGG) signal transduction category. We identified a list of signaling pathway gene signatures that were positively enriched in MAOB-OE PrSC cells with statistical significance (fig. S10A). Several of these pathways are well known to exert a paracrine-acting effect on stromal-epithelial interactions, including the pathways governed by neurotrophins, insulin, ErbB, vascular endothelial growth factor (VEGF), Wnt, and chemokines. Then, we conducted quantitative polymerase chain reaction (qPCR) screening in three pairs of MAOB-manipulated PrSC or PCF2 cells of the primary secreted factors of these pathways that are abundantly expressed in the stroma and have a stroma-initiated paracrine function enhancing stromal-epithelial interactions (*45*–*66*). We identified *CXCL12* (α-isoform, denoted as CXCL12 hereafter) as the top candidate because of its relatively larger differences and consistent pattern of expression changes in response to MAOB across all three cell pairs compared to other genes (fig. S10B). CXCL12, also known as stromal cell–derived factor 1 (SDF1), is a member of the C-X-C family of chemokines that can be secreted by stromal cells and exhibit elevated expression in CAFs of multiple tumor types including PC. Stromal-derived CXCL12 serves as a paracrine effector and binds to tumor-expressed C-X-C chemokine receptor type 4 (CXCR4) and CXCR7, which are both G protein–coupled receptors, to activate divergent downstream signaling pathways promoting PC growth and dissemination (*11*, *67*, *68*). In addition to the chemokine signaling pathway gene signature from the KEGG database, GSEA also revealed a chemotaxis gene signature positively enriched in MAOB-OE PrSC cells (Fig. 5A). We demonstrated lower levels of CXCL12 protein secretion in the culture media of MAOB-KD PrSC cells compared to controls (Fig. 5B). As opposed to MAOB, we found that MAOA exerted a suppressive effect on *CXCL12* expression in PrSC cells (fig. S10C). To determine whether the identified MAOB-CXCL12 axis in stromal cells could be recapitulated in the clinical setting, we assessed MAOB and CXCL12 protein levels in serial sections of a human PC TMA by IHC. Consistent with previous reports (*69*, *70*) and our findings above (fig. S1), MAOB and CXCL12 were found to be expressed in both tumor and stromal cells. Examining the stromal compartment specifically, we demonstrated a positive relationship of protein levels between stroma-expressed MAOB and CXCL12 in the TMA (Pearson's $r = 0.38$, $P < 0.05$, $n = 37$) (Fig. 5C). This was reinforced by a similar positive coexpression correlation between *MAOB* and *CXCL12* mRNA in additional public clinical datasets of stromal gene expression in cultured prostatic stromal cells (GSE34312, Pearson's $r = 0.46$, $P < 0.05$, $n = 20$) and laser-capture microdissected breast tumor stroma (GSE9014, Pearson's $r = 0.37$, $P < 0.01$, $n = 53$) (Fig. 5D), emphasizing the clinical relevance of the MAOB-CXCL12 connection in the stroma. These results in sum implicated CXCL12 as a potential mediator of stromal MAOB function in PC.

Next, we sought to find out how MAOB activates CXCL12 in PC stroma. We previously reported that MAOA activates Twist1, a basic helix-loop-helix transcription factor, via a ROS-driven signaling cascade to support MAOA function in PC cells. Mechanistically, MAOA produces ROS via oxidative deamination to stabilize hypoxia-inducible factor 1α (HIF1α) protein and subsequently induce the VEGF-A–mediated AKT/FOXO1 pathway, resulting in the nuclear export of transcription repressor FOXO1 to activate *TWIST1* transcription and gene expression (*14*). This led us to surmise that MAOB may also induce Twist1 as a key downstream effector in prostate stromal cells, possibly through the same ROS-dictated mechanism shared with MAOA given their similarity in multiple aspects as isoenzymes. To prove this idea, we demonstrated that MAOB OE in PrSC and PNF1 cells up-regulated, while MAOB KD in PrSC and PCF2 cells down-regulated, HIF1α protein and *VEGFA* mRNA (fig. S11, A and B). Analyzing a human PC TMA by co-IF staining, we revealed a positive correlation of protein levels between MAOB and HIF1α expressed in the tumor stroma (Pearson's $r = 0.43$, $P < 0.05$, $n = 20$) (fig. S11C), which is consistent with the previously identified coexpression correlation between MAOB and HIF1α in human gliomas (*71*). Moreover, MAOB OE in PrSC and PNF1 cells activated, while MAOB silencing in PrSC and PCF2 cells reduced, AKT and FOXO1 protein phosphorylation and Twist1 protein levels (fig. S11D). We also showed that forced expression of a constitutively active FOXO1 expression construct (AAA *FOXO1*) decreased MAOB-induced Twist1 protein levels in PrSC and PNF1 cells, while small interfering RNA (siRNA)–based KD of FOXO1 rescued Twist1 protein levels repressed by MAOB silencing in PrSC and PCF2 cells (fig. S11, E and F). To determine a direct connection of Twist1 with ROS in the stromal MAOB context, we demonstrated that NAC treatment reversed MAOB-activated Twist1 protein expression, whereas addition of H_2O_2 restored Twist1 protein levels down-regulated by MAOB KD in PrSC cells (Fig. 6A). Furthermore, unlike WT MAOB, forced expression of MAOB (Y435S) mutant deficient in ROS production did not induce *TWIST1* mRNA expression in PrSC cells (fig. S11G). These data in aggregate indicated ROS-dependent MAOB activation of Twist1 in prostate stromal cells. In addition, we found that pretreatment of MAOB-OE PrSC cells with *TWIST1* siRNA suppressed the proliferation of cocultured

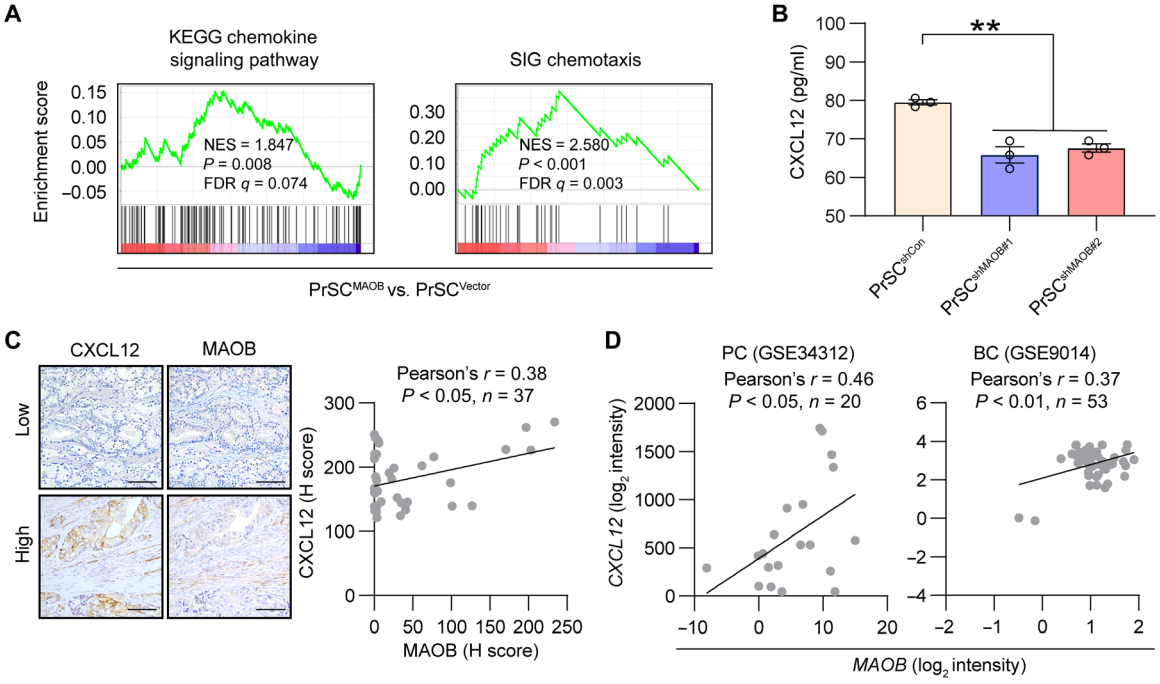

Fig. 5. MAOB activates CXCL12 in prostate tumor stroma. (**A**) GSEA plots of "chemokine signaling pathway" and "chemotaxis" gene sets enriched in MAOB-OE PrSC cells compared with controls. (**B**) ELISA of CXCL12 secretion in the culture media of control and MAOB-KD PrSC cells ($n = 3$). (**C**) Representative IHC images and corresponding Pearson's correlation analysis of stroma-expressed MAOB and CXCL12 protein levels in a PC TMA ($n = 37$). Scale bars, 100 μm. (**D**) Pearson's correlation analysis of *MAOB* and *CXCL12* mRNA levels in patient-derived cultured prostatic stromal cells (left, $n = 20$) and laser-capture microdissected breast tumor stroma (right, $n = 53$) from GSE34312 and GSE9014 datasets, respectively. Statistical analysis was performed using one-way ANOVA with Dunnett's test in (B). Data represent means ± SEM. $^{**}P < 0.01$.

PC-3 cells, suggesting that Twist1 mediates MAOB induction of a protumorigenic stromal phenotype (fig. S11H).

To determine whether Twist1 mediates MAOB regulation of CXCL12, we showed that Twist1 KD reverted MAOB-induced CXCL12 protein secretion and mRNA levels in PrSC cells. In parallel, NAC treatment in the context of MAOB, which reduced the levels of ROS as an upstream inducer of Twist1, corroborated these findings (Fig. 6, B and C). Conversely, forced expression of Twist1 restored *CXCL12* mRNA to control levels in MAOB-silenced PrSC cells (Fig. 6C). We also found the same trend of changes in *TWIST1* and *CXCL12* mRNA levels by OE or KD of MAOB in PNFs and PCFs, respectively (fig. S11, I and J). Furthermore, in contrast to WT MAOB, forced expression of a MAOB (Y435S) mutant that was unable to produce ROS and activate *TWIST1* failed to induce *CXCL12* mRNA in PrSC cells (fig. S11G). These results suggested that MAOB regulates CXCL12 at the transcriptional level likely in a Twist1-dependent manner in stromal cells. To explore the possible underlying transcriptional machinery, we analyzed the 0.7-kb human *CXCL12* promoter sequence with bioinformatical search tools for predicting putative transcription factor–binding sites and identified a putative Twist1-binding E-box site, CAGGTG (-514/-509) (*72*), in the proximal region of *CXCL12* promoter. We also found two putative Smad-binding elements (SBEs), AGAC (−570/−567) and GTCT (−564/−561) (*73*), located in close proximity to the E-box site on *CXCL12* promoter, which are able to bind an activated Smad complex by forming inverted repeats (*74*). These findings raised the possibility that TGFβ1-dependent Smads under MAOB's control may also contribute to *CXCL12* transcription in stromal cells.

To examine the effects of Twist1 and TGFβ1 on *CXCL12* transcription, we found that forced expression of Twist1 but not TGFβ1 treatment increased *CXCL12* mRNA levels in PrSC cells. Intriguingly, combined Twist1 and TGFβ1 treatment resulted in significantly higher induction of *CXCL12* mRNA in PrSC cells compared to either single treatment (Fig. 6D). We also observed a similar response of 0.7-kb *CXCL12* promoter Luc reporter to single or combination treatment with Twist1 and TGFβ1 in PrSC cells (Fig. 6E). Next, we inserted the 171–base pair (bp) E-box/SBE-centric promoter sequence upstream of the minimal promoter-driven Luc gene to construct a *CXCL12* E-box/SBE-Luc reporter and generated a series of reporters with the E-box, the SBEs, or both mutated. Unlike the WT reporter that was induced by Twist1 and/or TGFβ1 treatment in a similar trend as *CXCL12* mRNA and 0.7-kb promoter, mutating the E-box alone or the E-box and SBEs together rendered the reporters no longer responsive to either individual or combination treatment with Twist1 and TGFβ1, while mutating the SBEs alone retained the reporter inducible to Twist1 as well as to Twist1 and TGFβ1 in combination to a comparable extent in PrSC cells (Fig. 6F). These data support a model in which TGFβ1-dependent Smads induce *CXCL12* transcription by synergizing with Twist1 to enhance Twist1 transactivation activity. Following previous studies demonstrating the capability of Smads to interact with other transcription factors such as Snail to synergistically regulate target gene transcription and expression (*75*), we hypothesized that Smads may form a transcriptional complex with Twist1 to cooperatively activate *CXCL12* transcription. To test this hypothesis, we first performed a proximity ligation assay to assess whether Twist1 interacts with the

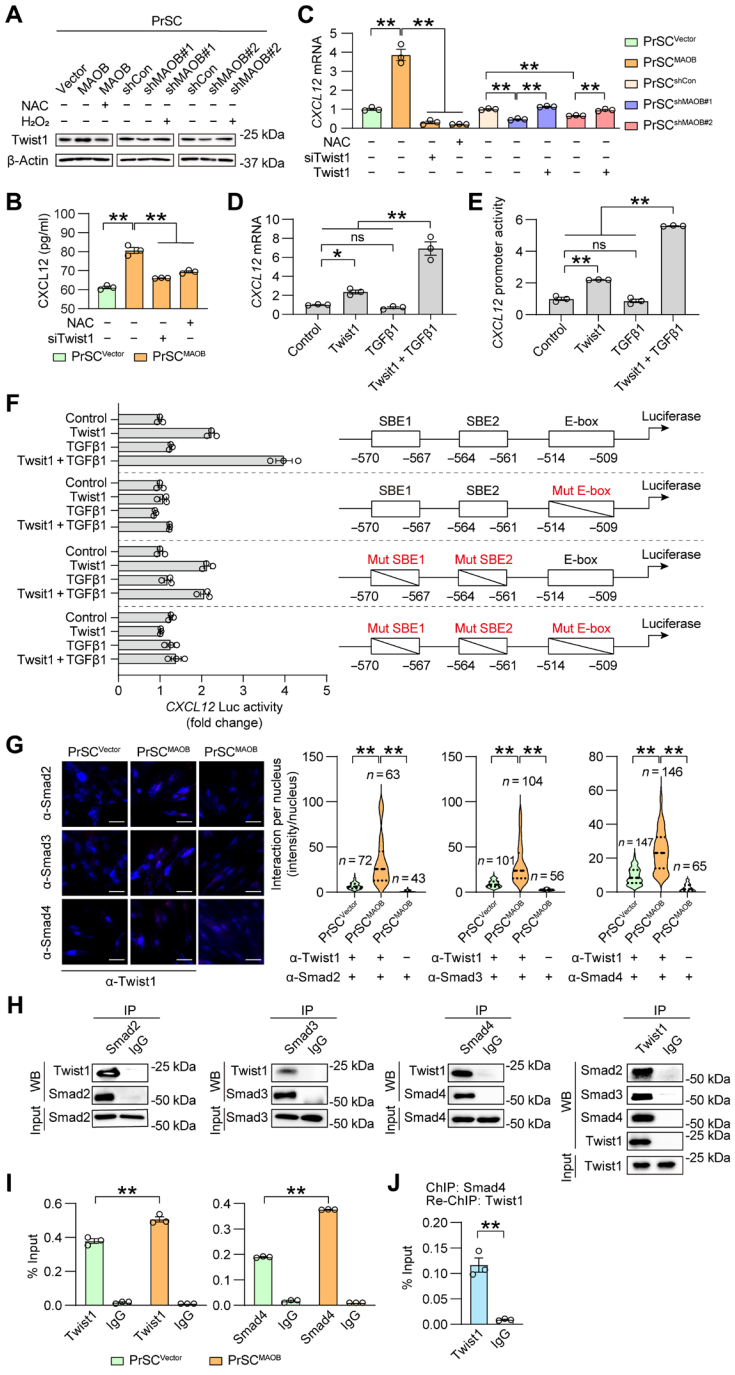

Fig. 6. MAOB induces *CXCL12* transcription and expression through Twist1 synergizing with TGFβ1/Smads in prostate stromal cells. (**A**) Western blot of Twist1 in control and MAOB-manipulated PrSC cells upon NAC (5 mM, 48 hours) or H_2O_2 (40 μM, 24 hours) treatment. (**B**) ELISA of CXCL12 secretion in culture media of control and MAOB-OE PrSC cells treated with *TWIST1* siRNA or NAC (5 mM, 48 hours) ($n = 3$). (**C**) qPCR of *CXCL12* in indicated PrSC cells upon NAC treatment (5 mM, 48 hours) or Twist1/*TWIST1* siRNA expression ($n = 3$). (**D** and **E**) Determination of *CXCL12* mRNA (D) and 0.7-kb promoter activity (E) in PrSC cells upon Twist1 expression and/or TGFβ1 treatment (10 ng/ml, 12 hours) ($n = 3$). (**F**) Schematic diagrams of WT and mutated *CXCL12* E-box/SBE-Luc constructs and determination of their activities in PrSC cells upon Twist1 expression and/or TGFβ1 treatment (10 ng/ml, 12 hours) ($n = 3$). (**G**) Representative proximity ligation assay staining and quantitation of indicated Twist1-Smad interactions by per-nucleus fluorescence intensity in control and MAOB-OE PrSC cells. Smad antibody incubation alone served as negative control. Numbers of nuclei included for comparisons between groups are denoted. Scale bars, 50 μm. (**H**) Co-IP assays of indicated Twist1-Smad interactions in PrSC cells with coexpression of Twist1 and individual Smads. Immunoglobulin G (IgG) was used in IP as negative control. Ten percent input was blotted as positive control. (**I**) ChIP analysis of chromatin from control and MAOB-OE PrSC cells precipitated with anti-Twist1, anti-Smad4, or a control IgG, followed by qPCR probing the E-box/SBE-centric *CXCL12* promoter region ($n = 3$). (**J**) ChIP analysis of chromatin from PrSC cells precipitated with anti-Smad4 antibody and then reprecipitated with anti-Twist1 or a control IgG (re-ChIP), followed by qPCR probing the E-box/SBE-encompassing *CXCL12* promoter sequence ($n = 3$). Statistical analysis was performed using one-way ANOVA with Tukey's test. Data represent means ± SEM. *$P < 0.05$, **$P < 0.01$; ns, not significant.

three Smads, where Smad4 forms a heteromeric complex with Smad2 or Smad3 in the nucleus to bind regulatory sequences of target genes (*76*). In situ assays visualized endogenous Twist1-Smad2, Twist1-Smad3, and Twist1-Smad4 protein complexes in PrSC cells, with 2.6- to 4.9-fold increases of Twist1-Smad interactions in the nucleus upon MAOB OE (Fig. 6G). We also performed a co-immunoprecipitation (IP) assay confirming that Twist1 physically interacts with all three Smads in PrSC cells (Fig. 6H). To assess direct occupancy of Twist1 and Smad4 as a representative Smad on *CXCL12* promoter, we performed a ChIP assay and found that Twist1 and Smad4 occupied the region encompassing their binding elements on *CXCL12* promoter in PrSC cells, with the occupancy enhanced upon MAOB OE (Fig. 6I). We further performed a ChIP–re-ChIP assay and demonstrated that Twist1 and Smad4 formed a complex on the E-box/SBE-centric region of *CXCL12* promoter in PrSC cells (Fig. 6J). Together, these results demonstrated that MAOB activates CXCL12 through Twist1 synergizing with TGFβ1-induced Smads for transcriptional up-regulation of *CXCL12* in prostate stromal cells.

MAOB promotes PC stromal-epithelial interactions and aggressive tumor behavior via the CXCL12/CXCR4 paracrine axis

Since our results nominated CXCL12 as a candidate paracrine factor underlying stromal MAOB function, we sought to determine whether CXCL12 in conjunction with its cognate receptors CXCR4 and CXCR7 mediates MAOB-elicited stromal-epithelial interactions. Coculturing PrSC and PC cells, we showed that inhibition of CXCL12 by a neutralizing antibody reversed the proliferation of C4-2 and PC-3 cells stimulated by MAOB-OE PrSC cells compared to controls. Parallel incubation of the anti-CXCL12 antibody with PC cells cultured alone demonstrated minimal effect on epithelial proliferation, eliminating the interference of a potential autocrine effect from tumor-derived CXCL12 with epithelial proliferation in cocultures (Fig. 7A). Conversely, we found that adding recombinant CXCL12 (rCXCL12) protein restored the proliferation of C4-2 and PC-3 cells suppressed by MAOB-KD PrSC cells in cocultures compared to controls (Fig. 7B). To investigate whether tumor-derived CXCL12 receptors engage in MAOB-dictated stromal-epithelial cross-talk, we silenced CXCR4 and CXCR7 individually by siRNA with their KD confirmed by Western blots in C4-2 and PC-3 cells (Fig. 7C), which were then subjected to cocultures with PrSC cells. We found that KD of CXCR4 but not CXCR7 in C4-2 and PC-3 cells blunted their proliferative response to MAOB-OE or KD PrSC cells in cocultures relative to controls. Furthermore, addition of rCXCL12 rescued CXCR7-KD C4-2 and PC-3 cell proliferation repressed by cocultured MAOB-silenced PrSC cells relative to controls but failed to do so with CXCR4-KD PC cells (Fig. 7, D and E). Consistently, we showed that treatment with AMD3100, a small-molecule CXCR4 antagonist, reduced the proliferation of C4-2 and PC-3 cells in coculture with MAOB-OE PrSC cells relative to controls (Fig. 7F). These results suggested that CXCR4 is the dominant CXCL12 receptor used by epithelial cells for connecting with stromal-derived MAOB/CXCL12 signaling to influence epithelial proliferation. The lessened ability of CXCR7 to confer a pro-proliferative effect of stromal MAOB/CXCL12 on epithelial cells in cocultures might be due to its nature as a scavenger receptor as well as its role assisting CXCR4 to trigger G protein–mediated intracellular signaling (*68*). To assess the migratory and invasive behavior of PC cells in response to stromal MAOB/CXCL12, we demonstrated that treatment with a CXCL12-neutralizing antibody or AMD3100 decreased epithelial cell migration and invasion induced by cocultured MAOB-OE PrSC cells compared to controls (Fig. 7G). Conversely, adding rCXCL12 restored the epithelial cell migration suppressed by MAOB-silenced PrSC cells to control levels in cocultures (Fig. 7H). Furthermore, treating C4-2 and PC-3 cells with rCXCL12 induced cell invasion to a similar extent as caused by MAOB-OE PrSC cells in cocultures compared to controls (as in Fig. 3F) (fig. S12A).

Next, we sought to elucidate the signaling pathways evoked by stromal MAOB via the CXCL12/CXCR4 axis in PC cells. To this end, we performed an unbiased proteomic screen using a cancer signaling phospho-antibody array featuring 269 highly specific antibodies important to cancer signaling pathways. We compared signaling protein levels in PC-3 cells treated with CM of MAOB-OE versus control PrSC cells. On the basis of stringent selection criteria (fold change > 1.5, $P < 0.05$), we identified a plethora of proteins, including p-Src (Tyr^{419}), p-caspase 9 (Ser^{196}), p-CREB (Ser^{133}), p-c-Kit (Tyr^{721}), p–Janus kinase 1 (JAK1) (Tyr^{1022}), p-BAD (Ser^{112}), and p–c-Jun N-terminal kinase (JNK) (Thr^{183}), whose phosphorylation was up-regulated in PC-3 cells by stromal MAOB and demonstrated a positive impact on epithelial growth by either enhancing proliferation or repressing apoptosis (Fig. 7I). Then, we performed independent Western blots and validated phosphorylation increases for Src, JNK, and CREB but not others in PC-3 cells exposed to CM of MAOB-OE PrSC cells versus controls, which was mirrored by their decreased phosphorylation in PC-3 cells treated with CM of MAOB-silenced PrSC cells versus controls (fig. S12, B and C). To further determine whether these proteins act downstream of CXCR4 in epithelial cells in the stromal MAOB context, we showed that CXCR4 KD attenuated the stromal MAOB–induced phosphorylation of Src and JNK but not CREB in PC-3 cells, while treatment with rCXCL12 rescued Src and JNK phosphorylation repressed by stromal MAOB silencing in PC-3 cells (Fig. 7, J and K, and fig. S12D). Consistent with the above findings pointing out CXCR4 as the dominant receptor conveying the effect of MAOB/CXCL12 paracrine signaling in epithelial cells, we demonstrated that KD of CXCR7 had no effect on stromal MAOB induction of Src and JNK phosphorylation in PC-3 cells (fig. S12E). Furthermore, we showed that pretreatment of C4-2 and PC-3 cells with Src inhibitor 1 or SP600125, small-molecule inhibitors of Src and JNK, respectively, before initiating stromal-epithelial cell cocultures led to complete blockade of stromal MAOB induction of epithelial proliferation, suggesting that both Src and JNK confer the protumorigenic effect of the MAOB/CXCL12-CXCR4 axis (Fig. 7L). Last, we determined the potential contributions of CXCL12-CXCR4/Src/JNK signaling to stromal MAOB's impact on the cancer cell expression of multiple genes involved in different mechanisms for anti-AR therapy resistance as shown above. We demonstrated that antagonizing the CXCL12-CXCR4/Src/JNK signaling by blocking agents against individual proteins of the axis suppressed the mRNA levels of most of those genes as induced in C4-2 cells exposed to CM of MAOB-OE PrSC cells compared to controls (fig. S12F). Together, these data demonstrated that stromal-derived MAOB promotes PC epithelial cell proliferation, migration, and invasion by activating the paracrine CXCL12-CXCR4/Src/JNK signaling pathway.

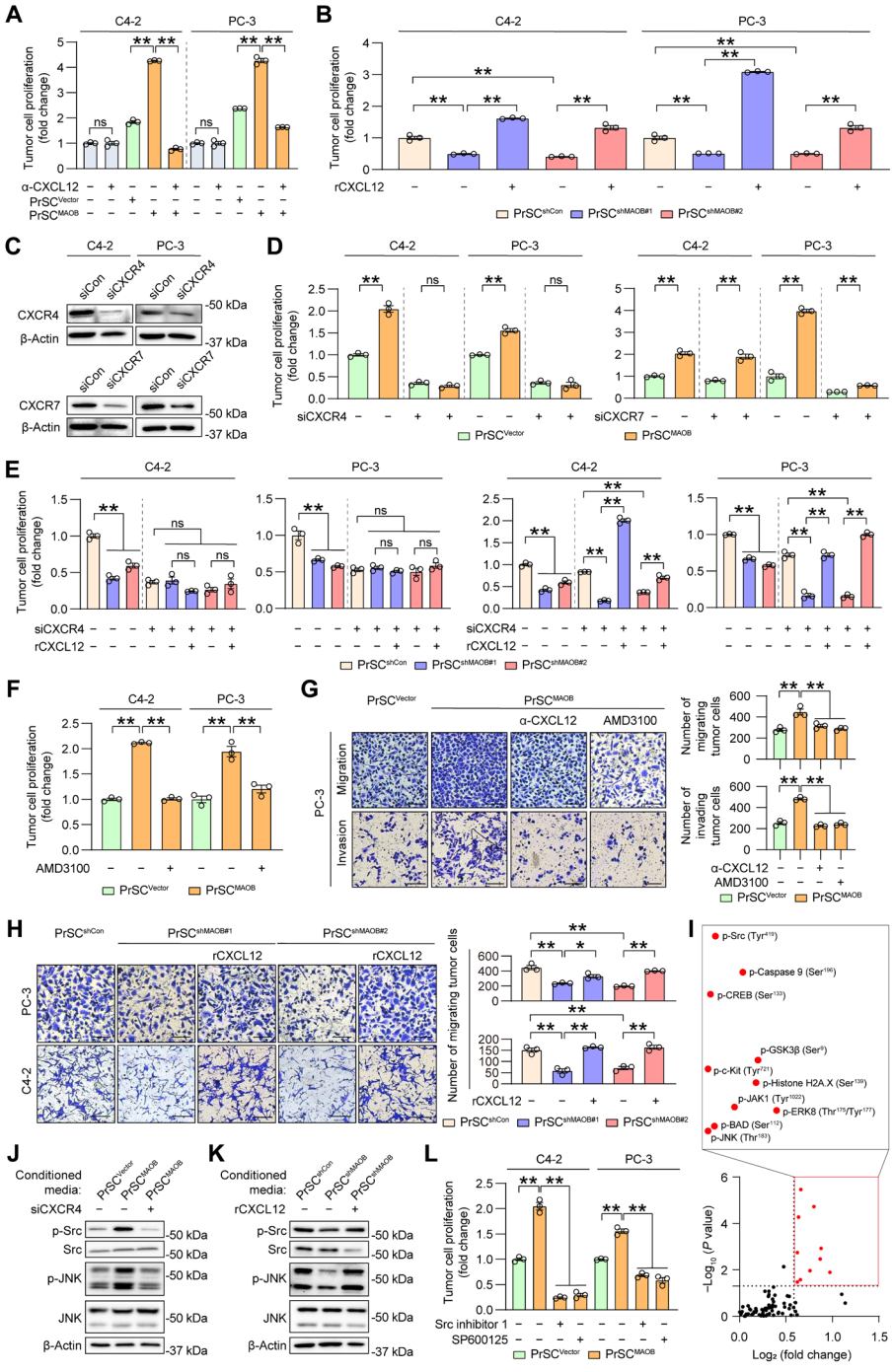

Fig. 7. Stromal MAOB promotes PC cell proliferation, migration, and invasion via CXCL12-CXCR4/Src/JNK paracrine signaling. (**A**) Quantitation of C4-2 and PC-3 PC cells in monoculture and coculture with indicated PrSC fibroblasts upon anti-CXCL12 (0.1 μg/ml) antibody treatment ($n = 3$). (**B**) Quantitation of PC cells in coculture with indicated PrSC cells treated with rCXCL12 protein (50 ng/ml; $n = 3$). (**C**) Western blot of CXCR4 and CXCR7 in control and CXCR4-KD/CXCR7-KD PC cells. (**D** and **E**) Quantitation of control and CXCR4-KD/CXCR7-KD PC cells in coculture with indicated PrSC cells treated without (D) or with (E) rCXCL12 (50 ng/ml; $n = 3$). (**F**) Quantitation of PC cells in coculture with indicated PrSC cells treated with 10 nM AMD3100 ($n = 3$). (**G**) Representative images and quantitation of PC-3 cell migration and invasion in coculture with indicated PrSC cells upon treatment with anti-CXCL12 antibody (0.1 μg/ml) or 10 nM AMD3100 ($n = 3$). Scale bars, 200 μm. (**H**) Representative images and quantitation of PC cell migration in coculture with indicated PrSC cells treated with rCXCL12 (50 ng/ml; $n = 3$). Scale bars, 100 μm. (**I**) Phospho-antibody array analysis of PC-3 cells treated with indicated PrSC cell CM. All phosphoprotein levels were normalized to their total forms from a single array with six replicate spots, with significantly activated phosphoproteins (fold change > 1.5, $P < 0.05$) denoted. (**J**) Western blot of p-Src and p-JNK in control and CXCR4-KD PC-3 cells treated with indicated PrSC cell CM. (**K**) Western blot of p-Src and p-JNK in PC-3 cells treated with indicated PrSC cell CM plus rCXCL12 (50 ng/ml). (**L**) Quantitation of PC cells in coculture with indicated PrSC cells following pretreatment with 40 nM Src inhibitor 1 or 10 μM SP600125 for 24 hours ($n = 3$). Statistical analysis was performed using one-way ANOVA with Tukey's test. Data represent means ± SEM. *$P < 0.05$, **$P < 0.01$; ns, not significant.

Pharmacological inhibition of MAOB in the tumor stroma restricts PC tumor growth in mice

Given the clinical availability of MAOB inhibitors (*13*), we sought to evaluate the therapeutic potential of targeting stromal MAOB to limit PC growth. To this end, we first determined the effectiveness of selegiline, a selective small-molecule MAOB inhibitor currently applied in the clinic to treat depression and early-stage Parkinson's disease (*77*), for suppressing PC cell growth in stromal-epithelial cell cocultures. We showed that selegiline treatment abolished the growth advantages of C4-2 and PC-3 cells in coculture with MAOB-OE PrSC cells relative to controls, which was paralleled by undetectable changes in the proliferation of C4-2 and PC-3 cells cultured alone upon selegiline treatment (Fig. 8A). Similarly, selegiline treatment inhibited the growth of C4-2 and PC-3 cells in coculture with mouse CAFs but not in monoculture (fig. S13A). We further found substantially lower MAOB protein levels in these PC cells compared to stromal cells (fig. S13, B and C), which is likely to render PC cells in monoculture insensitive to selegiline treatment compared to their response in coculture with stromal cells. These data in aggregate suggested that selegiline inhibits PC cell growth in stromal-epithelial cell cocultures through a cell-nonautonomous mechanism dependent on stromal MAOB inactivation.

Next, we established an orthotopic xenograft tumor model by inoculating Luc-tagged PC-3 cells into the prostates of immunodeficient male mice. After mice started to show visible development of tumor growth in prostates as examined by bioluminescence imaging (BLI), we treated mice with saline or selegiline at gradually increasing doses (0.5, 2, and 10 mg/kg) in a stroma-targeted manner given that the growth of PC-3 cells in monoculture was not affected by selegiline. Compared to the progressive growth of control tumors, we found that selegiline treatment dose-dependently suppressed prostate tumor growth in mice with significance reached starting at the dose of 2 mg/kg throughout a 6-week monitoring period, with an up to 78% reduction in tumor burden by BLI as well as tumor weighing at the experimental end point (Fig. 8, B to D). We also demonstrated that selegiline inhibited MAOB enzymatic activity in a dose-dependent manner without interference with MAOA activity in mouse liver where both isoforms distribute equally at the end point, confirming the specificity of selegiline (Fig. 8E). Consistent with tumor growth profiles, IHC analysis revealed dose-dependent decreases in Ki-67$^+$ tumor cell percentage, stromal expression of αSMA and CXCL12, and tumor expression of p-Src and p-JNK in treated tumors compared to controls (Fig. 8F). In addition, selegiline treatment at all doses did not alter mouse body weights (Fig. 8G). We also harvested vital organs including liver and kidneys for histopathological examination and collected blood from mice for liver and kidney function tests by measurement of a panel of markers [alanine aminotransferase (ALT), aspartate aminotransferase (AST), blood urea nitrogen (BUN), and creatinine]. We found no significant pathological and functional changes in liver and kidneys between any selegiline-treated and control groups (Fig. 8, H to L).

In summary, our preclinical studies suggest that up-regulated MAOB expression in the prostate stromal fibroblasts fosters stromal reprogramming toward a reactive state and consequently facilitates the acquisition of aggressive behavior by adjacent prostate tumor cells through a mechanism dictated by ROS-dependent synergistic interplay between Twist1 and TGFβ1/Smads to activate CXCL12/CXCR4 paracrine signaling, thereby driving stromal-epithelial interactions and prostate tumor growth and progression. Our results support repurposing a clinically used MAOB inhibitor to inactivate MAOB in the tumor stroma to disengage the interactive paracrine signaling network and disrupt stromal-tumor communication as a potential therapy for PC (Fig. 8M).

DISCUSSION

This study presented the first evidence that activation of MAOB in the stromal fibroblasts of the tumor microenvironment supports PC growth and progression by promoting stromal transition to a reactive protumorigenic state and stimulating the paracrine CXCL12/CXCR4 signaling axis to drive stromal-epithelial interactions. We demonstrated that pharmacological inactivation of stromal MAOB with a clinically used MAOB-selective inhibitor is a feasible and effective approach for PC intervention in an orthotopic xenograft model. Other than stromal MAOB's influence on PC tumors, we also provided hints for MAOB up-regulation in prostate stroma, which could be attributed in part to tumor-secreted factors (e.g., TNFα and IL-6) known to promote a CAF phenotype during the initial stage of communication between normal stromal and tumor cells. Additional potential stromal MAOB–activating inducers and signals from tumor cells and other cells within the tumor microenvironment also merit further exploration.

Tumor cells are codependent and coevolve with the surrounding stroma in the tumor microenvironment to receive growth stimuli and nutrients necessary for development into a fully malignant and aggressive stage (*8*, *36*). Thus, stroma-targeted therapeutic strategies have the potential to achieve antitumor efficacy by disrupting stromal-tumor communication. Especially in PC, prostatic CAFs are considered relatively genetically stable with evidence of excluding somatic mutations (*78*) and are thus an ideal therapeutic target with reduced risk of therapy resistance and tumor recurrence. Currently, most PC therapies in clinical use or trials emphasize tumor cell targeting and neglect the tumor-supportive stroma, resulting in limited survival benefits, especially in patients with relapsed disease. Filling this gap, we showed that stromal MAOB affects castration-resistant and metastatic epithelial proliferation regardless of the distinct intrinsic characteristics of different PC cells. We also demonstrated that stromal MAOB modulates the efficacy of anti-AR therapies such as ENZ in both sensitive and resistant PC cells, accompanied by corresponding changes in the expression levels of diverse underlying mechanistic regulators. These findings provide insights into developing a therapeutic strategy targeting MAOB in the tumor stroma as a likely generic approach bypassing tumor heterogeneity to complement malignant cell–targeted therapies for better therapeutic outcomes in advanced PC.

Our findings identified cellular redox under the control of MAOB in the stroma as a central mediator of reactive stroma formation. Supporting this idea, our interference and rescue experiments with the use of chemical redox modulators demonstrated the direct impact of MAOB-dependent ROS on stromal marker expression, ECM remodeling, and PC cell growth. This was reinforced by our observations that a MAOB enzyme-dead mutant incapable of ROS production failed to induce a reactive stroma in contrast to WT MAOB. ROS acts as a double-edged sword in a dose-dependent manner in stromal cell biology as well as in determination of tumor cell fate (*79*). We showed that enhanced ROS production in MAOB-activated stromal fibroblasts did not adversely perturb stromal cell

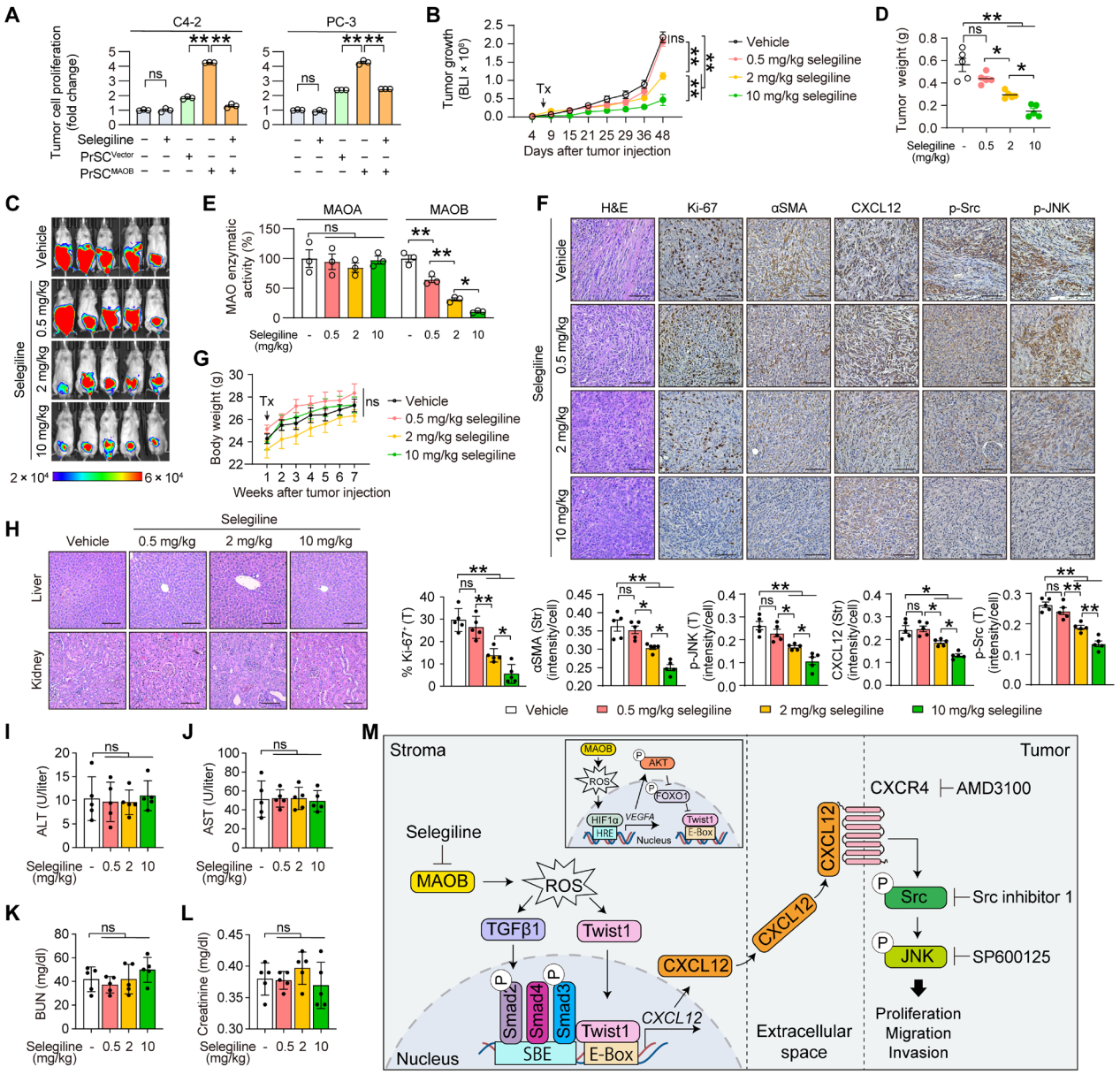

Fig. 8. Pharmacological inhibition of MAOB in stromal cells restricts PC growth in mice. (**A**) Quantitation of C4-2 and PC-3 cell proliferation in monoculture and coculture with control and MAOB-OE PrSC cells upon selegiline treatment (10 nM, 72 hours) ($n = 3$). (**B**) BLI-based growth curves of Luc-tagged PC-3 tumors grown in the prostates of male NSG mice treated with selegiline at various doses (0.5, 2, and 10 mg/kg) or saline as a vehicle ($n = 5$ per group). (**C**) BLI images of mice from each group at the end point. (**D**) Determination of tumor weights ($n = 5$). (**E**) Determination of MAOA and MAOB enzymatic activities in mouse liver tissue from each group at the end point ($n = 3$). (**F**) Representative images of H&E and IHC staining of tumor-expressed Ki-67, p-Src, and p-JNK and stroma-expressed αSMA and CXCL12 and their quantitation in tumor samples from each group ($n = 5$). Scale bars, 100 μm. (**G**) Mouse body weights determined weekly ($n = 5$). (**H**) Representative H&E images of mouse liver and kidney tissue from each group. Scale bars, 100 μm. (**I** to **L**) ELISA of ALT (I), AST (J), BUN (K), and creatinine (L) in mouse sera at the end point ($n = 5$). (**M**) Schematic depicting stromal-derived MAOB activation of paracrine CXCL12-CXCR4/Src/JNK signaling through interplay between ROS-dependent Twist1 (via a HIF1α/VEGF-A/AKT/FOXO1 pathway) and TGFβ1/Smads to promote stromal-epithelial interactions for PC growth and progression. Statistical analysis was performed using one-way ANOVA with Tukey's test in (A), (D) to (F), and (I) to (L) and two-way ANOVA with Tukey's test in (B) and (G). Data represent means ± SEM. $^*P < 0.05$, $^{**}P < 0.01$; ns, not significant.

growth and survival but rather conferred a proinflammatory and protumorigenic phenotype, suggesting that the potentially excessive levels of ROS produced by MAOB up-regulation may not be high enough to trigger a cell death pathway in stromal fibroblasts. We established that MAOB induces activation of Twist1/TGFβ1-dependent CXCL12 signaling in a ROS-dependent manner in stromal fibroblasts. These MAOB effectors have been reported to enhance cellular oxidative stress through diverse mechanisms in both normal and cancerous circumstances. For example, TGFβ signaling has been shown to increase mitochondrial ROS production in various cell types via different mechanisms (*80*, *81*). CXCL12 was also demonstrated to induce ROS generation through NADPH (reduced form of nicotinamide

adenine dinucleotide phosphate) oxidases to promote endothelial cell migration and angiogenesis (*82*). Thus, the reciprocal interplay of ROS with MAOB-downstream effectors may constitute a possible vicious cycle in the MAOB context to progressively achieve a level sufficient to convert naïve stroma to a reactive tumor-supportive phenotype. This model may also explain in part the minimal effect of MAOB activation on the fitness of stromal cells, as stromal cells would be able to gradually adapt to increasing levels of ROS to avoid acute cell injury and death.

One of the salient mechanistic features in this study is the discovery of Twist1- and TGFβ1/Smad-induced synergistic transcriptional activation of *CXCL12* in prostate stromal cells. Analogous to the mechanism of MAOA's role in PC epithelial cells (*14*), we found that Twist1 is activated by MAOB via ROS and becomes an effective regulatory node for MAOB action in prostate stromal cells, which coincides with previous findings that Twist1 is sufficient to drive CAF marker expression and tumor-supporting features in gastric cancer (*83*). Consistent with prior reports (*83*, *84*), we showed that Twist1 is recruited to an E-box site on *CXCL12* promoter to stimulate *CXCL12* gene transcription and expression in prostate stromal cells. An inverse regulatory relationship between Twist1 and CXCL12 was demonstrated in pulmonary mesenchymal cells (*85*). These opposing results suggest that Twist1 regulation of CXCL12 may be context dependent. In addition, we showed that MAOB-induced TGFβ1/Smad signaling acts as a catalyst to boost Twist1 transactivation of *CXCL12*, which is achieved by a synergism between Twist1 and Smads forming a transcriptional complex on *CXCL12* promoter. In contrast, our results indicate a marginal effect of TGFβ1 signaling on *CXCL12* transcription. Many studies have reported cross-talk and interplay between TGFβ1 and CXCL12 in stromal cells to cooperatively promote tumor progression, albeit with few clear clues to the underlying molecular mechanism (*11*, *86*). Our findings suggest a mechanism by which TGFβ signaling activates CXCL12 and potentially other stromal factors in a manner dependent on specific stromal active transcription factors like Twist1 in stromal cells.

Comparing in vitro and in vivo data, we noted that using selegiline in a stroma-targeted manner resulted in more reductions in prostate tumor growth in mice than PC cell growth in stromal-epithelial cell cocultures. One possible explanation could be that MAOB from other microenvironmental sources in addition to stromal fibroblasts may contribute to tumor growth. Another reasonable speculation could be that MAOB in the stromal fibroblasts may facilitate the participation of other types of stromal cells to cooperatively regulate tumor growth. For example, CAF-secreted CXCL12 was demonstrated to enhance angiogenesis by recruiting endothelial progenitor cells into carcinomas such as BC for tumor promotion (*67*). This appears to be a possible mechanism involved in stromal MAOB activation of tumor cell growth in mice but not in stromal-epithelial cell cocultures, thus likely accounting for the stronger inhibitory effect of selegiline in vivo than in vitro. These ideas need follow-up investigation and validation in more sophisticated models, such as tissue-specific conditional MAOB-KO mouse models and multicellular coculture systems comprising cancer, fibroblast, and other types of cells (e.g., endothelial cells).

Despite our findings demonstrating stromal MAOB's clinical and functional importance in PC, we recognize several limitations of our study. First, we manipulated MAOB levels in human fibroblast PrSC cells to generate a tissue recombinant xenograft mouse model for assessment of stromal MAOB's role in tumor growth. Although such an in vivo approach has been well documented in previous similar PC studies using either PrSC cells (*30*, *31*) or other human prostate fibroblast cells (*54*) to address the stromal impact on tumor growth, we did not take into account the viability of human fibroblasts following xenograft establishment in mice as well as the potential impact of mouse fibroblasts attracted by human xenografts on tumor growth. Our mouse study would definitely be strengthened by distinguishing and characterizing the individual state and role of human fibroblasts implanted and mouse fibroblasts recruited in mediating stromal MAOB's effect on tumor growth using stromal cell labeling and tracking methods. Second, we used several established human fibroblast cell lines in our study, which were also commonly used in prior studies addressing stromal-epithelial cross-talk in PC (*19*, *30*, *31*). However, their precise composition with regard to fibroblast subtypes and reactive status is not yet fully known. Future efforts are thus required for a more careful and comprehensive examination of the potential heterogeneities in different aspects of these fibroblast cell lines as well as their association with stromal MAOB expression and function in PC. Last, selegiline is known to have undesired side effects, which have been partially resolved, such as elimination of the dietary restrictions, by the recent development of transdermal delivery of selegiline (*77*). Despite pharmaceutical advances improving the safety of clinical MAOB inhibitors, additional studies are warranted to better characterize and optimize the type of dosing and delivery of selegiline and potentially other MAOB inhibitors necessary to achieve an anticancer effect with an acceptable safety profile in preclinical models and clinical trials.

MATERIALS AND METHODS

Clinical specimens

The TMAs for MAOB evaluation in Fig. 1 (A and B) and fig. S1 (A to D) and MAOA and MAOB expression patterns in fig. S2 (A and B) were obtained from PC tissue array PR1211 (US Biomax) containing 97 cases of prostate adenocarcinoma and 12 cases of normal prostate tissue with a single core and 1.5-mm-diameter size. The TMA for MAOB evaluation and association with clinical outcomes in Figs. 1C and 2 (D and E) and fig. S3 (D and E) was obtained from the NYU site of the Prostate Cancer Biorepository Network (PCBN), which originally contained 204 cases of prostate adenocarcinoma with two to six replicate cores per patient, with cohort characteristics summarized in table S1. Tissue cores for some cases in the NYU TMA were detached or wrinkled during the preparation process, leaving 195 cases from the NYU cohort for MAOB IHC staining. The castration-resistant (n = 16) and hormone-naïve (n = 38) PC TMAs for evaluation of stromal MAOB and adjacent epithelial CHGA in Fig. 2 (A and B) were constructed by the Biobank of Taipei General Veterans Hospital, as reviewed and approved by the Institutional Review Board (IRB) of Taipei General Veterans Hospital with written informed consent provided by patients. The TMA for evaluation of stromal MAOB–CXCL12 association in Fig. 5C was obtained from PC tissue array PR483c (US Biomax) containing 40 cases of prostate adenocarcinoma with a single core and 1.5-mm-diameter size. The TMAs for evaluation of stromal MAOB association with NE markers in fig. S3A and stromal MAOB–HIF1α association in fig. S11C were obtained from PC tissue array PR482a (US Biomax) containing 24 cases of prostate adenocarcinoma with duplicated cores and 1.5-mm-diameter size. Tissue cores for some

cases from TMAs PR483c and PR482a were lost during the staining process.

Cell lines and cell culture

Human PC PC-3 (CRL-1435) and DU145 (HTB-81), mouse PC TRAMP-C2 (CRL-2731), and human embryonic kidney 293T (CRL-3216) cell lines were obtained from the American Type Culture Collection. The human PC C4-2 cell line, mouse PC MPC3 and Pten-KO/Kras-OE cell lines, and three matched pairs of patient-derived prostatic normal (PNF1-3)– and cancer (PCF1-3)–associated primary fibroblast cell lines (*19*) were provided by L. W. K. Chung (Cedars-Sinai Medical Center). The ENZ-resistant C4-2B cell line, C4-2B^{ENZR}, was generated as described previously (*32*). The normal human prostate stromal fibroblast cell line PrSC was obtained from Lonza. The mouse NPF and prostatic CAF cell lines were provided by P. Roy-Burman (University of Southern California) and cultured as described previously (*87*). All human cell lines were authenticated by short tandem repeat profiling, regularly tested for *Mycoplasma* by the MycoProbe Mycoplasma Detection Kit (R&D Systems, CUL001B), and used with the number of cell passages kept below 10. Human PC cells were cultured in RPMI 1640 medium (Corning) supplemented with 10% fetal bovine serum (FBS; Atlanta Biologicals) and 1% penicillin-streptomycin (Corning). C4-2B^{ENZR} cells were cultured further in the continuous presence of 20 μM ENZ. 293T and mouse PC cells were cultured in Dulbecco's modified Eagle's medium (DMEM) (Corning) supplemented with 10% FBS and 1% penicillin-streptomycin. Human and mouse stromal fibroblast cells were cultured in T medium (Thermo Fisher Scientific) supplemented with 10% FBS and 1% penicillin-streptomycin.

Plasmids and reagents

A human *MAOB* lentiviral expression construct was generated by inserting the human *MAOB* coding region at EcoRI/XhoI sites in pLVX-AcGFP1-N1 vector (Clontech) containing a puromycin-resistant gene. The human *MAOB* (Y435S) mutant lentiviral expression construct was generated using a QuikChange II Site-Directed Mutagenesis Kit (Agilent Technologies, E200524) following the manufacturer's instructions, with WT construct used as a template. The primer sequence for mutagenesis is 5′-CACACTGGAGCGGCAG-CATGGAGGGGGCTG-3′ (mutated nucleotides underlined). A Dox-inducible *MAOB* shRNA expression construct was generated by inserting a human *MAOB* shRNA sequence from TRCN0000046019 at NheI/EcoRI sites in EZ-Tet-pLKO-Puro vector (Addgene) containing a puromycin-resistant gene. Primer sequences for constructing *MAOB* shRNA oligomers are forward 5′-CTAGCCCCAGAATCGT-ATCTTGAGATTACTAGTATCTCAAGATACGATTC-TGGGTTTTTG-3′ and reverse 5′-AATTCAAAAACCCAGAA-TCGTATCTTGAGATACTAGTAATCTCAAGATACGA-TTCTGGGG-3′. The human *TWIST1* expression construct was provided by A. Firulli (Indiana University). The human constitutively active AAA *FOXO1* expression construct was provided by K. -L. Guan (University of California, San Diego) and obtained from Addgene. The human 0.7-kb *CXCL12* promoter *Firefly* Luc reporter construct was provided by A. Caruz (University of Jaen, Spain). A human 171-bp *CXCL12* E-box/SBE-containing promoter *Firefly* Luc reporter construct (*CXCL12* E-box/SBE-Luc) was generated by inserting the corresponding promoter sequence upstream of a minimal promoter and the *Firefly* Luc gene of pGL4.26 vector (Promega). Primer sequences for cloning the sequence were forward 5′-AATCT-CGAGCTTTGTTTGTACAGGCGAGG-3′ and reverse 5′-CTCAA GCTTCTGCTTTCTGTGCGTGGG-3′. The pRL-TK *Renilla* Luc reporter was purchased from Promega. Human and mouse *MAOB* and nontarget control shRNA lentiviral particles were purchased from Sigma-Aldrich. Human *MAOB* siRNA pool (sc-35849), *TWIST1* siRNA pool (sc-38604), *CXCR4* siRNA pool (sc-35421), *CXCR7* siRNA pool (sc-94573), *MAOA* siRNA pool (sc-35847), *FOXO1* siRNA pool (sc-35382), and nontarget control siRNA (sc-37007) were purchased from Santa Cruz Biotechnology. Selegiline, NAC, H_2O_2, AMD3100, and Dox were purchased from Sigma-Aldrich. ENZ was purchased from MedChemExpress. Src inhibitor 1 was purchased from Selleck Chemicals. SP60025 was purchased from LC Laboratories. Human recombinant TGFβ1 and CXCL12 proteins were purchased from PeproTech. Human recombinant TNFα, IL-1α, and IL-6 proteins were purchased from Sino Biological.

Biochemical analyses

Total RNA was isolated using the RNeasy Mini Kit (Qiagen, 74104) and reverse-transcribed to cDNA by Moloney Murine Leukemia Virus reverse transcriptase (Promega) following the manufacturers' instructions. Subsequently, qPCR was conducted using SYBR Green PCR Master Mix and run with the Applied Biosystems QuantStudio 3 Real-Time PCR System (Thermo Fisher Scientific). PCR conditions included an initial denaturation step of 10 min at 95°C, followed by 40 cycles of PCR consisting of 15 s at 95°C and 1 min at 60°C. PCR data were analyzed by the $2^{-\Delta\Delta CT}$ method (*88*). Details on the primers used for qPCR are provided in table S2. For immunoblots, cells were extracted with radioimmunoprecipitation assay buffer in the presence of a protease/phosphatase inhibitor cocktail (Thermo Fisher Scientific). Blots were performed as described previously (*89*) using primary antibodies against MAOB (Sigma-Aldrich, HPA002328, RRID:AB_1854062), αSMA (Abcam, ab5694, RRID:AB_2223021), p-Smad2 (Ser$^{465/467}$) (Cell Signaling Technology, 3108, RRID:AB_490941), Smad2 (Cell Signaling Technology, 5339, RRID:AB_10626777), p-Smad3 (Ser$^{423/425}$) (Cell Signaling Technology, 9520, RRID:AB_2193207), Smad3 (Cell Signaling Technology, 9523, RRID:AB_2193182), Twist1 (Novus Biologicals, NBP2-37364, RRID:AB_2801339), CXCR4 (Santa Cruz Biotechnology, sc-9046), CXCR7 (GeneTex, GTX100027, RRID:AB_1240639), p-Src (Tyr^{419}) (Santa Cruz Biotechnology, sc-139601), Src (Santa Cruz Biotechnology, sc-8056, RRID:AB_627306), p-JNK (Thr^{183}/Tyr^{185}) (Cell Signaling Technology, 4668, RRID:AB_823588), JNK (Cell Signaling Technology, 9252, RRID:AB_2250373), p-caspase 9 (Ser^{196}) (Proteintech, 28794-1-AP, RRID:AB_2881214), caspase 9 (Proteintech, 10380-1-AP, RRID:AB_2068632), p-c-Kit (Tyr^{721}) (Signalway Antibody, 11240, RRID:AB_895204), c-Kit (Proteintech, 18696-1-AP, RRID:AB_2249558), p-JAK1 (Tyr^{1022}) (Novus Biologicals, NB100-82005, RRID:AB_1144529), JAK1 (Proteintech, 66466-1-Ig, RRID:AB_2881834), p-BAD (Ser^{112}) (Cell Signaling Technology, 5284, RRID:AB_560884), BAD (Proteintech, 10435-1-AP, RRID:AB_2061994), p-CREB (Ser^{133}) (Santa Cruz Biotechnology, sc-81486, RRID:AB_1125727), CREB (Cell Signaling Technology, 9197, RRID:AB_331277), HIF1α (BD Biosciences, 610959, RRID:AB_398272), p-AKT (Ser^{473}) (Cell Signaling Technology, 4060, RRID:AB_2315049), AKT (Cell Signaling Technology, 4691, RRID:AB_915783), p-FOXO1 (Ser^{256}) (Cell Signaling Technology, 9461, RRID:AB_329831), FOXO1 (Cell Signaling Technology, 2880, RRID:AB_2106495), or β-actin (Santa Cruz Biotechnology, sc-69879, RRID:AB_1123605). TGFβ1 (ELH-TGFb1-1) and

CXCL12 (DLH-SDF1a-1) protein levels in cell culture media were quantified by enzyme-linked immunosorbent assay (ELISA) (RayBiotech). Stromal MAOB target phosphoproteins expressed in PC cells were probed using a Cancer Signaling Phospho Antibody Array (Full Moon BioSystems, PCS248) following the manufacturer's instructions. MAOA and MAOB enzymatic activities in mouse liver tissue were measured with serotonin and benzylamine as substrates, respectively, by an EnzyChrom Monoamine Oxidase Assay Kit (BioAssay Systems, EMAO-100) following the manufacturer's instructions. Mouse serum levels of ALT (EALT-100), AST (EASTR-100), BUN (DIUR-100), and creatinine (DICT-500) were quantified by ELISA (BioAssay Systems).

Generation of stable OE and KD cells

Stable shRNA-mediated MAOB KD was achieved by infecting cells with lentivirus expressing human *MAOB* shRNA TRCN0000046019 (shMAOB#1, mainly used in this study and usually dubbed "shMAOB") or TRCN0000046021 (shMAOB#2) or mouse *Maob* shRNA TRCN0000076753 (shMaob#1) or TRCN0000076755 (shMaob#2) followed by puromycin (2 μg/ml) selection for 2 weeks to establish stable cell lines. A nontarget control shRNA was used as control for stable KD cells. Lentivirus production was performed for stable OE of MAOB or Dox-inducible *MAOB* shRNA in fibroblast cells. Briefly, 293T cells were cotransfected with a *MAOB*- or Dox-inducible *MAOB* shRNA–expressing lentiviral construct, pCMV delta R8.2 (Addgene), and pVSVG (Addgene) in a 4:2:1 ratio using Lipofectamine 2000 reagent (Thermo Fisher Scientific) following the manufacturer's instructions. The medium was changed 6 hours after transfection. The medium containing lentivirus was harvested 48 hours after transfection. Fibroblast cells were infected with lentivirus in the presence of polybrene (8 μg/ml) followed by 2-week puromycin selection. An empty lentiviral construct was used as control for stable MAOB OE in cells.

Analyses of tumor cell proliferation, apoptosis, migration, and invasion

For determining tumor cell proliferation in 2D coculture with fibroblasts as a coculture model primarily used in this study, 1×10^3 Luc- or fluorescence protein-tagged tumor cells were seeded over a monolayer of 2×10^4 fibroblast cells (tumor:fibroblast ratio, 1:20) in direct contact in 24-well plates to grow for 3 to 5 days. Tumor cell proliferation was determined by Luc readout using a luminometer or fluorescence readout by fluorescence microscopy. Fluorescence intensity was quantified by ImageJ software. Alternatively, Luc-tagged tumor cells were treated with CM of fibroblast cells for 3 to 5 days followed by determination of tumor cell proliferation by Luc readout. For determining stromal MAOB's effect on tumor cell proliferation in cocultures using an inducible KD system, fibroblasts expressing a Dox-inducible *MAOB* shRNA were treated with Dox (100 ng/ml) for 72 hours before tumor cell seeding, followed by determination of tumor cell proliferation. For determining the effects of stromal-derived ROS and Twist1 on tumor cell proliferation in cocultures, fibroblasts were treated with NAC or *TWIST1* siRNA for 24 hours before addition of tumor cells to establish cocultures, followed by determination of tumor cell proliferation. For determining the effect of stromal-derived MAOB/CXCL12-CXCR4 paracrine signaling on tumor cell proliferation in cocultures, selegiline, anti-CXCL12-neutralizing antibody (R&D Systems, MAB310, RRID:AB_2276927), rCXCL12 protein, or AMD3100 was added to cocultures 24 hours after tumor cell seeding, followed by determination of tumor cell proliferation. Parallel treatments of tumor cells cultured alone with selegiline or anti-CXCL12–neutralizing antibody were used as controls. For determining the effects of tumor-expressed CXCR4/CXCR7 and Src/JNK on tumor cell proliferation in cocultures, tumor cells were treated with *CXCR4* or *CXCR7* siRNA for 48 hours, or with Src or JNK inhibitors for 24 hours before seeding with fibroblasts to establish cocultures, followed by determination of tumor cell proliferation. For determining tumor cell proliferation in 3D coculture with fibroblasts, collagen gels were prepared by mixing 7 volumes of collage type 1 (4 mg/ml, Corning) with 1 volume of 10× DMEM, 1 volume of 1× DMEM, and 1 volume of FBS on ice. Reconstitution buffer (50 mM NaOH, 260 mM $NaHCO_3$, and 200 mM Hepes) was added dropwise for pH neutralization. Tumor cells were mixed with fibroblasts in a 1:3 ratio in the gel matrix. One milliliter of cell solution, including 3×10^5 tumor cells and 9×10^5 fibroblasts, was then added into a well of a 12-well plate. The gel was allowed to polymerize at 37°C for 1 hour followed by addition of complete medium. After 7 days, cells were dissociated from the gel with collagenase and dispersed for flow cytometric analysis of percentages of $EpCAM^+$ (an epithelial cell marker) tumor cells. For determining tumor cell migration and invasion in coculture with fibroblasts, 6.5-mm transwell inserts (8-μm pore size) coated with collagen I or growth factor–reduced Matrigel (Corning) were used. Tumor cells were serum-starved overnight before seeding. As a chemoattractant, 1×10^4 fibroblasts in serum-reduced medium were added to the bottom of lower chamber 24 hours before seeding of 5×10^4 tumor cells inside transwell inserts containing serum-free culture medium. After 24 to 48 hours, tumor cells that translocated to the lower surface of the insert filter were fixed in 4% formaldehyde. The fixed membranes were stained with 1% crystal violet. Assays were quantified by counting the number of stained nuclei in five independent fields in each transwell by ImageJ software. For determining stromal MAOB's effect on tumor cell invasion in cocultures using an inducible KD system, fibroblasts expressing a Dox-inducible *MAOB* shRNA were treated with Dox (100 ng/ml) for 72 hours before tumor cell seeding, followed by determination of tumor cell invasion. For determining the effect of stromal-derived CXCL12-CXCR4 paracrine signaling on tumor cell migration and invasion in cocultures, anti-CXCL12–neutralizing antibody, rCXCL12 protein, or AMD3100 were added concurrently with tumor cell seeding, followed by determination of tumor cell migration and invasion.

Analyses of stromal cell viability, proliferation, apoptosis, and senescence

Stromal fibroblast cells with shRNA- or siRNA-mediated KD of MAOB were assessed for cell viability and proliferation by multiple assays. For 3-(4,5-dimethylthiazol-2-yl)-5-(3-carboxymethoxyphenyl)-2-(4-sulfophenyl)-2H-tetrazolium (MTS) assays, cells were seeded in 96-well plates (2×10^3 cells per well) and grown for 5 days. Cells were then treated with MTS reagent for 30 min and proceeded with measurement of absorbance at 490 nm using an MTS cell proliferation assay kit (Abcam, ab197010). For cell cycle assays, cells were harvested and fixed in 70% ethanol at −20°C overnight. Fixed cells were then rinsed with cold phosphate-buffered saline (PBS) and incubated with 0.5 ml of propidium iodide/ribonuclease staining buffer (BD Biosciences) at room temperature for 15 min, followed by flow cytometric analysis of cell cycle phase distribution. For

5-bromo-2′-deoxyuridine (BrdU) assays, cells were incubated with BrdU for 6 hours and measured for absorbance at 450 nm using a BrdU cell proliferation ELISA kit (Abcam, ab126556). For determining MAOB's effect on stromal cell apoptosis, control and MAOB-KD stromal fibroblasts were fixed with 4% formaldehyde for 10 min at room temperature, rinsed twice with PBS, and permeabilized with 0.1% Triton X-100 solution for 10 min at room temperature followed by two washes with PBS. Subsequently, terminal deoxynucleotidyl transferase–mediated deoxyuridine triphosphate nick end labeling (TUNEL) staining was performed in cells using a fluorescein-based In Situ Cell Death Detection Kit (Sigma-Aldrich, 12156792910) following the manufacturer's instructions. DAPI (4′,6-diamidino-2-phenylindole) was added for nuclear staining before mounting. Images were acquired by fluorescence microscopy and analyzed for nuclear fluorescence with HALO (Indica Labs) software.

Analysis of PDX-derived organoid growth

Tumor tissues from LuCaP 147CR and LuCaP 93 advanced PC PDX models (*37*) were implanted into male 4- to 6-week-old NSG [nonobese diabetic SCID (severe combined immunodeficient) gamma] mice (The Jackson Laboratory, RRID:IMSR_JAX:005557) for expansion. The LuCaP 147CR tumor tissue was cut into ~5- to 10-mm^3 pieces and implanted subcutaneously into both flanks of the mice receiving surgical castration 2 weeks before implantation, while the LuCaP 93 tumor pieces were implanted subcutaneously into intact mice. Six weeks later, tumors were collected from the corresponding donor mice and subjected to digestion and seeding in 48-well plates (1×10^4 cells per well) with growth factor–reduced Matrigel for organoid culture following a published protocol (*90*). For determination of stromal MAOB's effect on organoid growth, established organoids were treated with CM of control and MAOB-manipulated fibroblasts, which were mixed 1:1 with complete medium, for 14 days with medium replenished every 3 days. Viability of the organoids was measured using a calcein AM dye–based LIVE/DEAD Viability/Cytotoxicity Kit (Thermo Fisher Scientific, L3224) and quantified by fluorescence microscopy following the manufacturer's instructions.

ROS measurement

Cells were washed with PBS and incubated with 5 μM CM-H_2DCFDA (Thermo Fisher Scientific) for 30 min. Cells were then trypsinized, and mean fluorescence reflecting cellular ROS levels was measured by flow cytometry or a microplate reader.

Collagen deposition assay

Collagen deposition was determined in PrSC cells with manipulated MAOB and ROS levels using a soluble collagen assay kit (Cell BioLabs, MET-5016) following the manufacturer's instructions. Briefly, cells were homogenized in lysis buffer containing 2.5% acetic acid and pepsin (0.1 mg/ml). The cell extracts were centrifuged at 12,000*g* for 10 min. The supernatant was neutralized with 2 N NaOH and transferred into a 96-well plate, followed by drying at 37°C overnight. Sirius Red reagent was added to the samples and standards to stain the collagen's triple-helix structure. The stained cells were washed with 5% acetic acid and incubated with extraction solution, followed by measurement of absorbance at 560 nm using a microplate reader.

Collagen gel contraction assay

Cell contraction was determined in PrSC cells with manipulated MAOB and ROS levels using a collagen-based cell contraction assay kit (Cell BioLabs, CBA-201) following the manufacturer's instructions. Briefly, cells were trypsinized and resuspended in complete medium at a density of 5×10^6 cells/ml. Cell suspensions were mixed with collagen gel working solution in a 1:4 ratio and plated into 48-well plates (250 μl per well). After incubation at 37°C for 1 hour, 500 μl of serum-free medium was added into each well. After 2 days, the gels were released from the side of the well. Gels were imaged every day, and cell contraction was assessed by measuring changes in the collagen gel size using ImageJ software.

Luc reporter assays

For determining the effect of Twist1 and TGFβ1 individually or in combination on *CXCL12* 0.7-kb promoter Luc reporter and WT and mutant *CXCL12* E-box/SBE-Luc reporters, PrSC cells were transfected with corresponding reporters together with *TWIST1* and pRL-TK plasmids and incubated for 24 hours, followed by treatment with recombinant TGFβ1 protein for another 12 hours. Cells were then harvested, and cell lysates were assayed for relative Luc activity by a Dual-Luciferase Reporter Assay (Promega, E1910) following the manufacturer's instructions.

ChIP- and re-ChIP–qPCR assays

ChIP-qPCR assays were used to determine the association of endogenous Twist1 and Smad4 proteins with an E-box and two SBEs on *CXCL12* promoter, respectively, in control and MAOB-OE PrSC cells treated with TGFβ1 (10 ng/ml) for 12 hours using a SimpleChIP Enzymatic Chromatin IP Kit (Cell Signaling Technology, 9002) following the manufacturer's instructions. Briefly, the chromatin was cross-linked with nuclear proteins, enzymatically digested with micrococcal nuclease followed by sonication, and immunoprecipitated with anti-Twist1, anti-Smad4 (Cell Signaling Technology, 46535, RRID:AB_2736998), or a normal immunoglobulin G (IgG, Cell Signaling Technology, 2729, RRID:AB_1031062). For further determining the association of a Twist1-Smad4 protein complex with the E-box/SBE-encompassing *CXCL12* promoter region, a re-ChIP–qPCR assay was performed using a Re-ChIP-IT Kit (Active Motif, 53016) following the manufacturer's instructions. Briefly, the chromatin eluted from the first ChIP assayed with anti-Smad4 antibody as described above was subjected to the second ChIP (re-ChIP) with anti-Twist1 or a normal IgG. The immunoprecipitates were pelleted with agarose beads, purified, and subjected to qPCR with primers specifically targeting the E-box/SBE-centric *CXCL12* promoter region. Primer sequences were forward 5′-GCTTTGTTTGTACAGGCGAGG-3′ and reverse 5′-CTGCTTTCTGTGCGTGGG-3′.

Proximity ligation assay

Cells were seeded on chamber slides and fixed with 4% formaldehyde for 10 min at room temperature, washed twice with PBS containing 0.02% Tween 20, and permeabilized with 0.5% Triton X-100/PBS solution (blocking solution) for 30 min at room temperature. Primary antibodies against Twist1 (mouse IgG), Smad2 (rabbit IgG), Smad3 (rabbit IgG), or Smad4 (rabbit IgG) were incubated in blocking solution at 4°C overnight. Assays were then performed with the Duolink In Situ Red Starter Kit Mouse/Rabbit (Sigma-Aldrich, DUO92101-1KT) according to the manufacturer's instructions

using anti-mouse MINUS and anti-rabbit PLUS proximity ligation assay probes. Images were acquired by a Zeiss Axio Imager M2 upright microscope using a ×40 objective and analyzed for fluorescence per nucleus with HALO software.

Co-IP assay

Twist1-Smad interactions in PrSC cells cotransfected with a *TWIST1* and an individual *SMAD* plasmid were determined using a Pierce Co-Immunoprecipitation Kit (Thermo Fisher Scientific, 26149) following the manufacturer's instructions. Briefly, cells were lysed in ice-cold IP lysis/wash buffer. An antibody against Twist1, Smad2, Smad3, Smad4, or a control IgG was immobilized for 2 hours using AminoLink Plus coupling resin for IP. One microgram of total protein lysates was immunoprecipitated with the resin at 4°C overnight. After incubation, the resin was washed and proteins in the immunoprecipitates were eluted and then subjected to immunoblotting analysis with antibodies against Twist1 or individual Smads.

Analysis of *CXCL12* promoter

Site-directed mutagenesis was used to mutate the E-box and SBEs on *CXCL12* E-box/SBE-Luc, with WT construct used as the template. Mutagenesis was carried out using a QuikChange II XL Site-Directed Mutagenesis Kit following the manufacturer's instructions. The primer sequences for mutating the E-box and SBEs were forward 5′-GCCGCAAGCCGGGTTGGTGGCGAGCTTG-3′ and reverse 5′-CGAGCCACGCTGACTGCAAACATGGCTTTCATTC-CCGCAGATCG-3′, respectively (mutated nucleotides underlined). Mutated nucleotides were verified by DNA sequencing before experimental use.

Animal studies

Male 4- to 6-week-old SCID (RRID:IMSR_TAC:CB17SC), NSG (RRID:IMSR_JAX:005557), and C57BL/6 (RRID:IMSR_JAX:000664) mice were purchased from Taconic or The Jackson Laboratory, housed in the animal research facilities at Cedars-Sinai Medical Center or Washington State University, and fed a normal chow diet. For determining stromal MAOB's effect on adjacent tumor growth in a tissue recombinant xenograft model, tissue recombinants were prepared following a published protocol (*91*) with minor adjustments of the tumor:fibroblast mix ratio and total number of cells for transplantation as described previously (*16*). Briefly, PC cells were mixed with fibroblast cells at a ratio of 1:3, with each recombinant composed of 2.5×10^5 Luc-tagged PC C4-2 cells and 7.5×10^5 control or MAOB-KD PrSC fibroblast cells. After polymerization with rat tail collagen, the cell-collagen mixture graft was overlaid with complete medium and incubated at 37°C overnight before transplantation. The grafts were transplanted under the renal capsule of anesthetized SCID mice to allow development of tumors ($n = 5$ mice per group). Tumor growth was monitored by BLI with a Xenogen IVIS Spectrum Imaging System (PerkinElmer) weekly for 8 weeks after transplantation. The photon flux in mouse kidneys was analyzed by Living Image software (PerkinElmer). BLI signal data were acquired after background subtraction. At the end point, tumors were dissected, weighed, and collected for subsequent analyses. For determining stromal Maob's effect on mouse prostate tumor growth in an immunocompetent mouse model, a mix of 1×10^5 Pten-KO/Kras-OE mouse PC cells with 3×10^5 control or Maob-KD mouse CAFs was injected subcutaneously into C57BL/6 mice ($n = 4$ mice per group). At the end point, tumors were dissected, weighed, and collected for subsequent analyses. For determining the effect of the MAOB inhibitor selegiline on tumor growth in an orthotopic xenograft model, 5×10^5 Luc-tagged PC-3 cells were mixed 1:1 with Matrigel and injected into the prostates of anesthetized NSG mice to develop prostate tumors. Mice were randomized into four groups to receive treatments with selegiline at various doses (0.5, 2, and 10 mg/kg) or saline as a vehicle ($n = 5$ mice per group) based on BLI signal in prostates 1 week after tumor injection. Daily intraperitoneal injections of selegiline were given for 6 weeks, with saline injection for the control group. Tumor growth was monitored by BLI weekly. At the experimental end point, tumors were dissected for analysis.

IHC and IF analyses

IHC and IF analyses of clinical prostate tumor and xenograft and allograft tumor samples were performed using antibodies against MAOB, CHGA (Santa Cruz Biotechnology, sc-393941, RRID:AB_2801371), SYP (Santa Cruz Biotechnology, sc-17750, RRID:AB_628311), Ki-67 (Cell Signaling Technology, 9027, RRID:AB_2636984), AR (Cell Signaling Technology, 5153, RRID:AB_10691711), αSMA, CXCL12 (R&D Systems, MAB350, RRID:AB_2088149), p-Src (Tyr^{419}), p-JNK (Thr^{183}/Tyr^{185}), or HIF1α following a published protocol (*14*). Serial TMA sections were used for IHC staining of two proteins separately as in Figs. 1 (A to C), 2B, and 5C. A single TMA was used for co-IF staining of two proteins simultaneously as in figs. S1 (C and D), S2 (A and B), and S11C. The IHC and IF data were quantitatively analyzed by assigning H score, cell-based intensity, or percentage of positive expression for individual protein staining by HALO software after areas of interest were defined using manual tissue segmentation by a pathologist.

For multiplex IF staining, all primary antibodies were tested as mono-staining before multiplex staining. Multiplex IF staining was performed using an Opal 6-Plex Detection Kit (Akoya Biosciences, NEL811001KT) following the manufacturer's protocol. Briefly, after deparaffinization and rehydration, antigen retrieval was performed by heat treatment using AR6 buffer. After cooling, nonspecific binding was blocked using antibody diluent/block for 10 min, followed by incubation with a primary antibody overnight at 4°C. Slides were then incubated with Opal polymer horseradish peroxidase for 10 min, followed by incubation with Opal fluorophores for 10 min. The antibody was stripped by heat treatment. The procedures above were repeated from the antigen retrieval step for each subsequent antibody. The primary antibodies against MAOB, SYP, and CHGA were sequentially used. Last, slides were counterstained with DAPI for 5 min and mounted using antifade mounting medium (VECTASHIELD). Tissue dots were scanned under Leica CMi8 confocal microscopy to obtain multispectral images for quantification using HALO software.

RNA-seq, single-cell RNA-seq, and bioinformatics analyses

The total RNA of control and MAOB-OE and KD PrSC cells was extracted by RNeasy Mini Kit and underwent deoxyribonuclease digestion following the manufacturer's instructions. RNA-seq was performed on an Illumina HiSeq 4000 at Novogene. Bowtie 2 v2.1.0 was used for mapping to the human genome hg19 transcript set. RSEM v1.2.15 was used to calculate the count and estimate the gene expression level. Trimmed mean of M-values (TMM) method in the edge R package was used for gene expression normalization. GSEA

v4.1.0 was used to evaluate the association of MAOB expression with response to wounding, ROS, TGFβ and chemokine signaling, and other pathways using relevant gene sets from the molecular signature database (MSigDB v7.4). The human PC (GSE34312) and BC (GSE9014) datasets of stromal gene expression used for different correlation studies or examination of stromal MAOB expression between different disease states were downloaded from the Oncomine or National Center for Biotechnology Information (NCBI) Gene Expression Omnibus (GEO) databases.

The single-cell RNA-seq raw data in GSE141445 and GSE137829 datasets were downloaded from the NCBI GEO database and analyzed using the R and Bioconductor packages. The basic quality metrics including unique molecular identifier (UMI) per cell and gene counts per cell were estimated using the scater package. Cells with low library size, low numbers of features, or a high number of mitochondrial genes were filtered out using the quickPerCellQC function in the scater package. The cutoffs for UMI and mitochondrial genes are 1000 and 10%, respectively. Batch effects were removed, and datasets from each sample were integrated using the fastMNN method in the bachelor R package. Hypervariable expressed genes were identified by the getTopHVGs function in the scran package. The top 500 genes with the highest biological variances were selected for dimension reduction using the TSNE algorithm. Clusters were identified using the buildSNNGraph function in the scran package. Literature-based marker genes were selected for categorizing different fibroblast subtypes.

Statistics

Data are presented as means ± SEM as indicated in figure legends. Comparisons between Kaplan-Meier curves were analyzed using the log-rank test. Correlations between groups were determined by Pearson correlation. All other comparisons were analyzed by unpaired two-tailed Student's *t* test, one-way analysis of variance (ANOVA) with Tukey's or Dunnett's multiple-comparison tests, or two-way ANOVA with Tukey's or Sidak's multiple-comparison test. A *P* value less than 0.05 was considered statistically significant.

Study approval

All animal studies received prior approval from the Institutional Animal Care and Use Committees (IACUCs) at Cedars-Sinai Medical Center and Washington State University and complied with IACUC recommendations. Human tissue samples were obtained from the NYU site of the PCBN and the Biobank of Taipei Veterans General Hospital under approved protocols from their local IRBs.

Supplementary Materials

This PDF file includes:

Figs. S1 to S13
Tables S1 and S2

REFERENCES AND NOTES

1. H. Sung, J. Ferlay, R. L. Siegel, M. Laversanne, I. Soerjomataram, A. Jemal, F. Bray, Global cancer statistics 2020: GLOBOCAN estimates of incidence and mortality worldwide for 36 cancers in 185 countries. *CA Cancer J. Clin.* **71**, 209–249 (2021).
2. D. A. Barron, D. R. Rowley, The reactive stroma microenvironment and prostate cancer progression. *Endocr. Relat. Cancer* **19**, R187–R204 (2012).
3. M. Kato, V. R. Placencio-Hickok, A. Madhav, S. Haldar, M. Tripathi, S. Billet, R. Mishra, B. Smith, K. Rohena-Rivera, P. Agarwal, F. Duong, B. Angara, D. Hickok, Z. Liu, N. A. Bhowmick, Heterogeneous cancer-associated fibroblast population potentiates neuroendocrine differentiation and castrate resistance in a CD105-dependent manner. *Oncogene* **38**, 716–730 (2019).
4. T. Eder, A. Weber, H. Neuwirt, G. Grünbacher, C. Ploner, H. Klocker, N. Sampson, I. E. Eder, Cancer-associated fibroblasts modify the response of prostate cancer cells to androgen and anti-androgens in three-dimensional spheroid culture. *Int. J. Mol. Sci.* **17**, 1458 (2016).
5. A. F. Olumi, G. D. Grossfeld, S. W. Hayward, P. R. Carroll, T. D. Tlsty, G. R. Cunha, Carcinoma-associated fibroblasts direct tumor progression of initiated human prostatic epithelium. *Cancer Res.* **59**, 5002–5011 (1999).
6. N. Dumont, B. Liu, R. A. Defilippis, H. Chang, J. T. Rabban, A. N. Karnezis, J. A. Tjoe, J. Marx, B. Parvin, T. D. Tlsty, Breast fibroblasts modulate early dissemination, tumorigenesis, and metastasis through alteration of extracellular matrix characteristics. *Neoplasia* **15**, 249–262 (2013).
7. F. Bonollo, G. N. Thalmann, M. Kruithof-de Julio, S. Karkampouna, The role of cancer-associated fibroblasts in prostate cancer tumorigenesis. *Cancers* **12**, 1887 (2020).
8. T. Valencia, J. Y. Kim, S. Abu-Baker, J. Moscat-Pardos, C. S. Ahn, M. Reina-Campos, A. Duran, E. A. Castilla, C. M. Metallo, M. T. Diaz-Meco, J. Moscat, Metabolic reprogramming of stromal fibroblasts through p62-mTORC1 signaling promotes inflammation and tumorigenesis. *Cancer Cell* **26**, 121–135 (2014).
9. F. Bruzzese, C. Hägglöf, A. Leone, E. Sjöberg, M. S. Roca, S. Kiflemariam, T. Sjöblom, P. Hammarsten, L. Egevad, A. Bergh, A. Ostman, A. Budillon, M. Augsten, Local and systemic protumorigenic effects of cancer-associated fibroblast-derived GDF15. *Cancer Res.* **74**, 3408–3417 (2014).
10. S. Memarzadeh, L. Xin, D. J. Mulholland, A. Mansukhani, H. Wu, M. A. Teitell, O. N. Witte, Enhanced paracrine FGF10 expression promotes formation of multifocal prostate adenocarcinoma and an increase in epithelial androgen receptor. *Cancer Cell* **12**, 572–585 (2007).
11. M. Ao, O. E. Franco, D. Park, D. Raman, K. Williams, S. W. Hayward, Cross-talk between paracrine-acting cytokine and chemokine pathways promotes malignancy in benign human prostatic epithelium. *Cancer Res.* **67**, 4244–4253 (2007).
12. J. C. Shih, K. Chen, M. J. Ridd, Monoamine oxidase: From genes to behavior. *Annu. Rev. Neurosci.* **22**, 197–217 (1999).
13. M. Bortolato, K. Chen, J. C. Shih, Monoamine oxidase inactivation: From pathophysiology to therapeutics. *Adv. Drug Deliv. Rev.* **60**, 1527–1533 (2008).
14. J. B. Wu, C. Shao, X. Li, Q. Li, P. Hu, C. Shi, Y. Li, Y.-T. Chen, F. Yin, C.-P. Liao, B. L. Stiles, H. E. Zhau, J. C. Shih, L. W. K. Chung, Monoamine oxidase A mediates prostate tumorigenesis and cancer metastasis. *J. Clin. Invest.* **124**, 2891–2908 (2014).
15. L. True, I. Coleman, S. Hawley, C. Y. Huang, D. Gifford, R. Coleman, T. M. Beer, E. Gelmann, M. Datta, E. Mostaghel, B. Knudsen, P. Lange, R. Vessella, D. Lin, L. Hood, P. S. Nelson, A molecular correlate to the Gleason grading system for prostate adenocarcinoma. *Proc. Natl. Acad. Sci. U.S.A.* **103**, 10991–10996 (2006).
16. J. Li, T. Pu, L. Yin, Q. Li, C. P. Liao, B. J. Wu, MAOA-mediated reprogramming of stromal fibroblasts promotes prostate tumorigenesis and cancer stemness. *Oncogene* **39**, 3305–3321 (2020).
17. D. Lavie, A. Ben-Shmuel, N. Erez, R. Scherz-Shouval, Cancer-associated fibroblasts in the single-cell era. *Nat. Cancer* **3**, 793–807 (2022).
18. D. Yang, J. Liu, H. Qian, Q. Zhuang, Cancer-associated fibroblasts: From basic science to anticancer therapy. *Exp. Mol. Med.* **55**, 1322–1332 (2023).
19. X. Sun, H. He, Z. Xie, W. Qian, H. E. Zhau, L. W. K. Chung, F. F. Marshall, R. Wang, Matched pairs of human prostate stromal cells display differential tropic effects on LNCaP prostate cancer cells. *In Vitro Cell. Dev. Biol. Anim* **46**, 538–546 (2010).
20. E. Sahai, I. Astsaturov, E. Cukierman, D. G. DeNardo, M. Egeblad, R. M. Evans, D. Fearon, F. R. Greten, S. R. Hingorani, T. Hunter, R. O. Hynes, R. K. Jain, T. Janowitz, C. Jorgensen, A. C. Kimmelman, M. G. Kolonin, R. G. Maki, R. S. Powers, E. Pure, D. C. Ramirez, R. Scherz-Shouval, M. H. Sherman, S. Stewart, T. D. Tlsty, D. A. Tuveson, F. M. Watt, V. Weaver, A. T. Weeraratna, Z. Werb, A framework for advancing our understanding of cancer-associated fibroblasts. *Nat. Rev. Cancer* **20**, 174–186 (2020).
21. M. Ricote, I. Garcia-Tunon, F. R. Bethencourt, B. Fraile, R. Paniagua, M. Royuela, Interleukin-1 (IL-1α and IL-1β) and its receptors (IL-1RI, IL-1RII, and IL-1Ra) in prostate carcinoma. *Cancer* **100**, 1388–1396 (2004).
22. G. Rodriguez-Berriguete, B. Sanchez-Espiridion, J. R. Cansino, G. Olmedilla, P. Martinez-Onsurbe, M. Sanchez-Chapado, R. Paniagua, B. Fraile, M. Royuela, Clinical significance of both tumor and stromal expression of components of the IL-1 and TNF-α signaling pathways in prostate cancer. *Cytokine* **64**, 555–563 (2013).
23. E. Giannoni, F. Bianchini, L. Masieri, S. Serni, E. Torre, L. Calorini, P. Chiarugi, Reciprocal activation of prostate cancer cells and cancer-associated fibroblasts stimulates epithelial-mesenchymal transition and cancer stemness. *Cancer Res.* **70**, 6945–6956 (2010).
24. Y. Sun, J. Niu, J. Huang, Neuroendocrine differentiation in prostate cancer. *Am. J. Transl. Res.* **1**, 148–162 (2009).
25. A. Aparicio, C. J. Logothetis, S. N. Maity, Understanding the lethal variant of prostate cancer: Power of examining extremes. *Cancer Discov.* **1**, 466–468 (2011).

26. I. V. Litvinov, D. J. Vander Griend, L. Antony, S. Dalrymple, A. M. De Marzo, C. G. Drake, J. T. Isaacs, Androgen receptor as a licensing factor for DNA replication in androgen-sensitive prostate cancer cells. *Proc. Natl. Acad. Sci. U.S.A.* **103**, 15085–15090 (2006).
27. J. L. Bishop, D. Thaper, S. Vahid, A. Davies, K. Ketola, H. Kuruma, R. Jama, K. M. Nip, A. Angeles, F. Johnson, A. W. Wyatt, L. Fazli, M. E. Gleave, D. Lin, M. A. Rubin, C. C. Collins, Y. Wang, H. Beltran, A. Zoubeidi, The master neural transcription factor BRN2 is an androgen receptor-suppressed driver of neuroendocrine differentiation in prostate cancer. *Cancer Discov.* **7**, 54–71 (2017).
28. D. A. Leach, G. Buchanan, Stromal androgen receptor in prostate cancer development and progression. *Cancers* **9**, 10 (2017).
29. A. Hiroto, W. K. Kim, A. Pineda, Y. He, D. H. Lee, V. Le, A. W. Olson, J. Aldahl, C. H. Nenninger, A. J. Buckley, G. Q. Xiao, J. Geradts, Z. Sun, Stromal androgen signaling acts as tumor niches to drive prostatic basal epithelial progenitor-initiated oncogenesis. *Nat. Commun.* **13**, 6552 (2022).
30. T. Ohishi, H. Abe, C. Sakashita, U. Saqib, M. S. Baig, S.-I. Ohba, H. Inoue, T. Watanabe, M. Shibasaki, M. Kawada, Inhibition of mitochondria ATP synthase suppresses prostate cancer growth through reduced insulin-like growth factor-1 secretion by prostate stromal cells. *Int. J. Cancer* **146**, 3474–3484 (2020).
31. M. Kawada, H. Inoue, T. Masuda, D. Ikeda, Insulin-like growth factor I secreted from prostate stromal cells mediates tumor-stromal cell interactions of prostate cancer. *Cancer Res.* **66**, 4419–4425 (2006).
32. C. Liu, W. Lou, Y. Zhu, J. C. Yang, N. Nadiminty, N. W. Gaikwad, C. P. Evans, A. C. Gao, Intracrine androgens and AKR1C3 activation confer resistance to enzalutamide in prostate cancer. *Cancer Res.* **75**, 1413–1422 (2015).
33. T. Bland, J. Wang, L. Yin, T. Pu, J. Li, J. Gao, T.-P. Lin, A. C. Gao, B. J. Wu, WLS-Wnt signaling promotes neuroendocrine prostate cancer. *iScience* **24**, 101970 (2021).
34. A. M. Chioni, R. Grose, FGFR1 cleavage and nuclear translocation regulates breast cancer cell behavior. *J. Cell Biol.* **197**, 801–817 (2012).
35. M. L. Henriksson, S. Edin, A. M. Dahlin, P. A. Oldenborg, A. Oberg, B. Van Guelpen, J. Rutegard, R. Stenling, R. Palmqvist, Colorectal cancer cells activate adjacent fibroblasts resulting in FGF1/FGFR3 signaling and increased invasion. *Am. J. Pathol.* **178**, 1387–1394 (2011).
36. R. Mishra, S. Haldar, V. Placencio, A. Madhav, K. Rohena-Rivera, P. Agarwal, F. Duong, B. Angara, M. Tripathi, Z. Liu, R. A. Gottlieb, S. Wagner, E. M. Posadas, N. A. Bhowmick, Stromal epigenetic alterations drive metabolic and neuroendocrine prostate cancer reprogramming. *J. Clin. Invest.* **128**, 4472–4484 (2018).
37. H. M. Nguyen, R. L. Vessella, C. Morrissey, L. G. Brown, I. M. Coleman, C. S. Higano, E. A. Mostaghel, X. Zhang, L. D. True, H.-M. Lam, M. Roudier, P. H. Lange, P. S. Nelson, E. Corey, LuCaP prostate cancer patient-derived xenografts reflect the molecular heterogeneity of advanced disease and serve as models for evaluating cancer therapeutics. *Prostate* **77**, 654–671 (2017).
38. M. Rotinen, S. You, J. Yang, S. G. Coetzee, M. Reis-Sobreiro, W. C. Huang, F. Huang, X. Pan, A. Yanez, D. J. Hazelett, C. Y. Chu, K. Steadman, C. M. Morrissey, P. S. Nelson, E. Corey, L. W. K. Chung, S. J. Freedland, D. Di Vizio, I. P. Garraway, R. Murali, B. S. Knudsen, M. R. Freeman, ONECUT2 is a targetable master regulator of lethal prostate cancer that suppresses the androgen axis. *Nat. Med.* **24**, 1887–1898 (2018).
39. S. Deng, C. Wang, Y. Wang, Y. Xu, X. Li, N. A. Johnson, A. Mukherji, U.-G. Lo, L. Xu, J. Gonzalez, L. A. Metang, J. Ye, C. R. Tirado, K. Rodarte, Y. Zhou, Z. Xie, C. Arana, V. Annamalai, X. Liu, D. J. Vander Griend, D. Strand, J.-T. Hsieh, B. Li, G. Raj, T. Wang, P. Mu, Ectopic JAK-STAT activation enables the transition to a stem-like and multilineage state conferring AR-targeted therapy resistance. *Nat. Cancer* **3**, 1071–1087 (2022).
40. P. A. Watson, V. K. Arora, C. L. Sawyers, Emerging mechanisms of resistance to androgen receptor inhibitors in prostate cancer. *Nat. Rev. Cancer* **15**, 701–711 (2015).
41. Á. Quintanal-Villalonga, J. M. Chan, H. A. Yu, D. Pe'er, C. L. Sawyers, T. Sen, C. M. Rudin, Lineage plasticity in cancer: A shared pathway of therapeutic resistance. *Nat. Rev. Clin. Oncol.* **17**, 360–371 (2020).
42. U. E. Martinez-Outschoorn, R. M. Balliet, D. B. Rivadeneira, B. Chiavarina, S. Pavlides, C. Wang, D. Whitaker-Menezes, K. M. Daumer, Z. Lin, A. K. Witkiewicz, N. Flomenberg, A. Howell, R. G. Pestell, E. S. Knudsen, F. Sotgia, M. P. Lisanti, Oxidative stress in cancer associated fibroblasts drives tumor-stroma co-evolution: A new paradigm for understanding tumor metabolism, the field effect and genomic instability in cancer cells. *Cell Cycle* **9**, 3256–3276 (2010).
43. R. M. Geha, K. Chen, J. Wouters, F. Ooms, J. C. Shih, Analysis of conserved active site residues in monoamine oxidase A and B and their three-dimensional molecular modeling. *J. Biol. Chem.* **277**, 17209–17216 (2002).
44. F. L. Miles, R. A. Sikes, Insidious changes in stromal matrix fuel cancer progression. *Mol. Cancer Res.* **12**, 297–312 (2014).
45. G. J. Ritfeld, A. Patel, A. Chou, T. L. Novosat, D. G. Castillo, R. A. C. Roos, M. Oudega, The role of brain-derived neurotrophic factor in bone marrow stromal cell-mediated spinal cord repair. *Cell Transplant.* **24**, 2209–2220 (2015).
46. Y. Wang, Y. Jing, L. Ding, X. Zhang, Y. Song, S. Chen, X. Zhao, X. Huang, Y. Pu, Z. Wang, Y. Ni, Q. Hu, Epiregulin reprograms cancer-associated fibroblasts and facilitates oral squamous cell carcinoma invasion via JAK2-STAT3 pathway. *J. Exp. Clin. Cancer Res.* **38**, 274 (2019).
47. T. Jarde, W. H. Chan, F. J. Rossello, T. Kaur Kahlon, M. Theocharous, T. Kurian Arackal, T. Flores, M. Giraud, E. Richards, E. Chan, G. Kerr, R. M. Engel, M. Prasko, J. F. Donoghue, S. I. Abe, T. J. Phesse, C. M. Nefzger, P. J. McMurrick, D. R. Powell, R. J. Daly, J. M. Polo, H. E. Abud, Mesenchymal niche-derived neuregulin-1 drives intestinal stem cell proliferation and regeneration of damaged epithelium. *Cell Stem Cell* **27**, 646–662.e7 (2020).
48. M. R. Freeman, S. Paul, M. Kaefer, M. Ishikawa, R. M. Adam, A. A. Renshaw, K. Elenius, M. Klagsbrun, Heparin-binding EGF-like growth factor in the human prostate: Synthesis predominantly by interstitial and vascular smooth muscle cells and action as a carcinoma cell mitogen. *J. Cell. Biochem.* **68**, 328–338 (1998).
49. C. Unger, N. Kramer, D. Unterleuthner, M. Scherzer, A. Burian, A. Rudisch, M. Stadler, M. Schlederer, D. Lenhardt, A. Riedl, S. Walter, A. Wernitznig, L. Kenner, M. Hengstschlager, J. Schuler, W. Sommergruber, H. Dolznig, Stromal-derived IGF2 promotes colon cancer progression via paracrine and autocrine mechanisms. *Oncogene* **36**, 5341–5355 (2017).
50. Y. Yokoyama, D. S. Charnock-Jones, D. Licence, A. Yanaihara, J. M. Hastings, C. M. Holland, M. Emoto, A. Sakamoto, T. Sakamoto, H. Maruyama, S. Sato, H. Mizunuma, S. K. Smith, Expression of vascular endothelial growth factor (VEGF)-D and its receptor, VEGF receptor 3, as a prognostic factor in endometrial carcinoma. *Clin. Cancer Res.* **9**, 1361–1369 (2003).
51. C. Muir, L. W. K. Chung, D. D. Carson, M. C. Farach-Carson, Hypoxia increases VEGF-A production by prostate cancer and bone marrow stromal cells and initiates paracrine activation of bone marrow endothelial cells. *Clin. Exp. Metastasis* **23**, 75–86 (2006).
52. K. Zins, A. Thomas, T. Lucas, M. Sioud, S. Aharinejad, D. Abraham, Inhibition of stromal PlGF suppresses the growth of prostate cancer xenografts. *Int. J. Mol. Sci.* **14**, 17958–17971 (2013).
53. E. Ogawa, K. Takenaka, K. Yanagihara, M. Kurozumi, T. Manabe, H. Wada, F. Tanaka, Clinical significance of VEGF-C status in tumour cells and stromal macrophages in non-small cell lung cancer patients. *Br. J. Cancer* **91**, 498–503 (2004).
54. Y. Sun, J. Campisi, C. Higano, T. M. Beer, P. Porter, I. Coleman, L. True, P. S. Nelson, Treatment-induced damage to the tumor microenvironment promotes prostate cancer therapy resistance through WNT16B. *Nat. Med.* **18**, 1359–1368 (2012).
55. K. Teiken, M. Kuehnel, J. Rehkaemper, H. Kreipe, F. Laenger, K. Hussein, D. Jonigk, Non-canonical WNT6/WNT10A signal factor expression in EBV+ post-transplant smooth muscle tumors. *Clin. Sarcoma Res.* **8**, 10 (2018).
56. T. Pukrop, F. Klemm, T. Hagemann, D. Gradl, M. Schulz, S. Siemes, L. Trumper, C. Binder, Wnt 5a signaling is critical for macrophage-induced invasion of breast cancer cell lines. *Proc. Natl. Acad. Sci. U.S.A.* **103**, 5454–5459 (2006).
57. L. Fu, C. Zhang, L.-Y. Zhang, S.-S. Dong, L.-H. Lu, J. Chen, Y. Dai, Y. Li, K. L. Kong, D. L. Kwong, X.-Y. Guan, Wnt2 secreted by tumour fibroblasts promotes tumour progression in oesophageal cancer by activation of the Wnt/β-catenin signalling pathway. *Gut* **60**, 1635–1643 (2011).
58. Q. Zhang, Y. Pan, J. Ji, Y. Xu, Q. Zhang, L. Qin, Roles and action mechanisms of WNT4 in cell differentiation and human diseases: A review. *Cell Death Discov.* **7**, 287 (2021).
59. S. Raghavan, P. Mehta, Y. Xie, Y. L. Lei, G. Mehta, Ovarian cancer stem cells and macrophages reciprocally interact through the WNT pathway to promote pro-tumoral and malignant phenotypes in 3D engineered microenvironments. *J. Immunother. Cancer* **7**, 190 (2019).
60. Y. Jung, J. K. Kim, Y. Shiozawa, J. Wang, A. Mishra, J. Joseph, J. E. Berry, S. McGee, E. Lee, H. Sun, J. Wang, T. Jin, H. Zhang, J. Dai, P. H. Krebsbach, E. T. Keller, K. J. Pienta, R. S. Taichman, Recruitment of mesenchymal stem cells into prostate tumours promotes metastasis. *Nat. Commun.* **4**, 1795 (2013).
61. B. K. K. Lo, M. Yu, D. Zloty, B. Cowan, J. Shapiro, K. J. McElwee, CXCR3/ligands are significantly involved in the tumorigenesis of basal cell carcinomas. *Am. J. Pathol.* **176**, 2435–2446 (2010).
62. S. M. Hald, Y. Kiselev, S. Al-Saad, E. Richardsen, C. Johannessen, M. Eilertsen, T. K. Kilvaer, K. Al-Shibli, S. Andersen, L. T. Busund, R. M. Bremnes, T. Donnem, Prognostic impact of CXCL16 and CXCR6 in non-small cell lung cancer: Combined high CXCL16 expression in tumor stroma and cancer cells yields improved survival. *BMC Cancer* **15**, 441 (2015).
63. M. Ammirante, S. Shalapour, Y. Kang, C. A. M. Jamieson, M. Karin, Tissue injury and hypoxia promote malignant progression of prostate cancer by inducing CXCL13 expression in tumor myofibroblasts. *Proc. Natl. Acad. Sci. U.S.A.* **111**, 14776–14781 (2014).
64. L. A. Begley, S. Kasina, R. Mehra, S. Adsule, A. J. Admon, R. J. Lonigro, A. M. Chinnaiyan, J. A. Macoska, CXCL5 promotes prostate cancer progression. *Neoplasia* **10**, 244–254 (2008).
65. Y. Lu, B. Dong, F. Xu, Y. Xu, J. Pan, J. Song, J. Zhang, Y. Huang, W. Xue, CXCL1-LCN2 paracrine axis promotes progression of prostate cancer via the Src activation and epithelial-mesenchymal transition. *Cell Commun. Signal* **17**, 118 (2019).
66. H. W. Cheng, L. Onder, J. Cupovic, M. Boesch, M. Novkovic, N. Pikor, I. Tarantino, R. Rodriguez, T. Schneider, W. Jochum, M. Brutsche, B. Ludewig, CCL19-producing fibroblastic stromal cells restrain lung carcinoma growth by promoting local antitumor T-cell responses. *J. Allergy Clin. Immunol.* **142**, 1257–1271.e4 (2018).
67. A. Orimo, P. B. Gupta, D. C. Sgroi, F. Arenzana-Seisdedos, T. Delaunay, R. Naeem, V. J. Carey, A. L. Richardson, R. A. Weinberg, Stromal fibroblasts present in invasive human breast

carcinomas promote tumor growth and angiogenesis through elevated SDF-1/CXCL12 secretion. *Cell* **121**, 335–348 (2005).
68. Y. Shi, D. J. Riese II, J. Shen, The role of the CXCL12/CXCR4/CXCR7 chemokine axis in cancer. *Front. Pharmacol.* **11**, 574667 (2020).
69. N. Gupta, H. Ochiai, Y. Hoshino, S. Klein, J. Zustin, R. R. Ramjiawan, S. Kitahara, N. Maimon, D. Bazou, S. Chiang, S. Li, D. H. Schanne, R. K. Jain, L. L. Munn, P. Huang, S. V. Kozin, D. G. Duda, Inhibition of CXCR4 enhances the efficacy of radiotherapy in metastatic prostate cancer models. *Cancers* **15**, 1021 (2023).
70. M. Parol-Kulczyk, A. Gzil, J. Ligmanowska, D. Grzanka, Prognostic significance of SDF-1 chemokine and its receptors CXCR4 and CXCR7 involved in EMT of prostate cancer. *Cytokine* **150**, 155778 (2022).
71. M. A. Sharpe, D. S. Baskin, Monoamine oxidase B levels are highly expressed in human gliomas and are correlated with the expression of HiF-1α and with transcription factors Sp1 and Sp3. *Oncotarget* **7**, 3379–3393 (2016).
72. A. T. Chang, Y. Liu, K. Ayyanathan, C. Benner, Y. Jiang, J. W. Prokop, H. Paz, D. Wang, H.-R. Li, X.-D. Fu, F. J. Rauscher III, J. Yang, An evolutionarily conserved DNA architecture determines target specificity of the TWIST family bHLH transcription factors. *Genes Dev.* **29**, 603–616 (2015).
73. L. Zawel, J. L. Dai, P. Buckhaults, S. Zhou, K. W. Kinzler, B. Vogelstein, S. E. Kern, Human Smad3 and Smad4 are sequence-specific transcription activators. *Mol. Cell* **1**, 611–617 (1998).
74. C. S. Hill, Transcriptional control by the SMADs. *Cold Spring Harb. Perspect. Biol.* **8**, a022079 (2016).
75. T. Vincent, E. P. A. Neve, J. R. Johnson, A. Kukalev, F. Rojo, J. Albanell, K. Pietras, I. Virtanen, L. Philipson, P. L. Leopold, R. G. Crystal, A. G. de Herreros, A. Moustakas, R. F. Pettersson, J. Fuxe, A SNAIL1-SMAD3/4 transcriptional repressor complex promotes TGF-beta mediated epithelial-mesenchymal transition. *Nat. Cell Biol.* **11**, 943–950 (2009).
76. Y. Shi, J. Massague, Mechanisms of TGF-beta signaling from cell membrane to the nucleus. *Cell* **113**, 685–700 (2003).
77. I. Miklya, The significance of selegiline/(-)-deprenyl after 50 years in research and therapy (1965-2015). *Mol. Psychiatry* **21**, 1499–1503 (2016).
78. D. Bianchi-Frias, R. Basom, J. J. Delrow, I. M. Coleman, O. Dakhova, X. Qu, M. Fang, O. E. Franco, N. G. Ericson, J. H. Bielas, S. W. Hayward, L. True, C. Morrissey, L. Brown, N. A. Bhowmick, D. Rowley, M. Ittmann, P. S. Nelson, Cells comprising the prostate cancer microenvironment lack recurrent clonal somatic genomic aberrations. *Mol. Cancer Res.* **14**, 374–384 (2016).
79. K. R. Martin, J. C. Barrett, Reactive oxygen species as double-edged swords in cellular processes: Low-dose cell signaling versus high-dose toxicity. *Hum. Exp. Toxicol.* **21**, 71–75 (2002).
80. C. H. Chang, S. Pauklin, ROS and TGFβ: From pancreatic tumour growth to metastasis. *J. Exp. Clin. Cancer Res.* **40**, 152 (2021).
81. R. M. Liu, L. P. Desai, Reciprocal regulation of TGF-β and reactive oxygen species: A perverse cycle for fibrosis. *Redox Biol.* **6**, 565–577 (2015).
82. X. Pi, L. Xie, A. L. Portbury, S. Kumar, P. Lockyer, X. Li, C. Patterson, NADPH oxidase-generated reactive oxygen species are required for stromal cell-derived factor-1α–stimulated angiogenesis. *Arterioscler. Thromb. Vasc. Biol.* **34**, 2023–2032 (2014).
83. K. W. Lee, S. Y. Yeo, C. O. Sung, S. H. Kim, Twist1 is a key regulator of cancer-associated fibroblasts. *Cancer Res.* **75**, 73–85 (2015).
84. A. Arthur, D. Cakouros, L. Cooper, T. Nguyen, S. Isenmann, A. C. W. Zannettino, C. A. Glackin, S. Gronthos, Twist-1 enhances bone marrow mesenchymal stromal cell support of hematopoiesis by modulating CXCL12 expression. *Stem Cells* **34**, 504–509 (2016).
85. J. Tan, J. R. Tedrow, M. Nouraie, J. A. Dutta, D. T. Miller, X. Li, S. Yu, Y. Chu, B. Juan-Guardela, N. Kaminski, K. Ramani, P. S. Biswas, Y. Zhang, D. J. Kass, Loss of Twist1 in the mesenchymal compartment promotes increased fibrosis in experimental lung injury by enhanced expression of CXCL12. *J. Immunol.* **198**, 2269–2285 (2017).
86. O. E. Franco, M. Jiang, D. W. Strand, J. Peacock, S. Fernandez, R. S. Jackson II, M. P. Revelo, N. A. Bhowmick, S. W. Hayward, Altered TGF-β signaling in a subpopulation of human stromal cells promotes prostatic carcinogenesis. *Cancer Res.* **71**, 1272–1281 (2011).
87. C. P. Liao, H. Adisetiyo, M. Liang, P. Roy-Burman, Cancer-associated fibroblasts enhance the gland-forming capability of prostate cancer stem cells. *Cancer Res.* **70**, 7294–7303 (2010).
88. K. J. Livak, T. D. Schmittgen, Analysis of relative gene expression data using real-time quantitative PCR and the $2^{-\Delta\Delta CT}$ method. *Methods* **25**, 402–408 (2001).
89. J. B. Wu, K. Chen, X. M. Ou, J. C. Shih, Retinoic acid activates monoamine oxidase B promoter in human neuronal cells. *J. Biol. Chem.* **284**, 16723–16735 (2009).
90. S. Ning, J. Zhao, A. P. Lombard, L. S. D'Abronzo, A. R. Leslie, M. Sharifi, W. Lou, C. Liu, J. C. Yang, C. P. Evans, E. Corey, H.-W. Chen, A. Yu, P. M. Ghosh, A. C. Gao, Activation of neural lineage networks and ARHGEF2 in enzalutamide-resistant and neuroendocrine prostate cancer and association with patient outcomes. *Commun. Med.* **2**, 118 (2022).
91. N. Cheng, D. L. Lambert, Mammary transplantation of stromal cells and carcinoma cells in C57BL/6J mice. *J. Vis. Exp.*, 2716 (2011).

Acknowledgments: We thank L. W. K. Chung (Cedars-Sinai Medical Center) for comprehensive support of this study, Y. Li (University of Southern California) for technical help, and G. Mawyer for editorial assistance. **Funding:** This work was supported by NIH/NCI grants R01CA258634 and R37CA233658 and WSU startup funding to B.J.W. and Department of Defense Prostate Cancer Research Program grants W81XWH-18-2-0013, W81XWH-18-2-0015, W81XWH-18-2-0016, W81XWH-18-2-0017, W81XWH-18-2-0018, and W81XWH-18-2-0019 to the Prostate Cancer Biorepository Network. The establishment and characterization of LuCaP PDX models were supported by the Pacific Northwest Prostate Cancer SPORE (P50CA097186), the Department of Defense Prostate Cancer Biorepository Network (W81XWH-14-2-0183), and NCI grant (P01CA163227). **Author contributions:** T.P. and B.J.W. conceived the study. T.P., J. Wei, A.Z., J.Z., J.C., L.Y., J.L., and B.J.W. performed experiments. T.P., J. Wang, and B.J.W. performed formal analysis. T.-P.L., J.M., E.C., and A.C.G. provided material support. B.J.W. provided project administration, wrote the manuscript, supervised the study, and acquired funding. **Competing interests:** E.C. received sponsored research funding from Sanofi, Gilead, AbbVie, Genentech, Janssen Research, AstraZeneca, GSK, Bayer Pharmaceuticals, Forma Pharmaceuticals, Foghorn, Kronos, and MacroGenics. The other authors declare no competing interests. **Data and materials availability:** All data needed to evaluate the conclusions in the paper are present in the paper and/or the Supplementary Materials. All reagents generated in this study are accessible from the corresponding author with a completed material transfer agreement. The RNA-seq raw sequence files generated and reported in this study are available in the NCBI GEO database with the accession number GSE188316.

Submitted 28 April 2023
Accepted 9 January 2024
Published 9 February 2024
10.1126/sciadv.adi4935